Methane mapping, emission quantification, and attribution in two European cities; Utrecht, NL and Hamburg, DE

Hossein Maazallahi[1,2], Julianne M. Fernandez[3], Malika Menoud[1], Daniel Zavala-Araiza[1,4], Zachary D. Weller[5], Stefan Schwietzke[6], Joseph C. von Fischer[7], Hugo Denier van der Gon[2], and Thomas Röckmann[1]

[1]Institute for Marine and Atmospheric research Utrecht (IMAU), Utrecht University (UU), Utrecht, The Netherlands
[2]Netherlands Organisation for Applied Scientific Research (TNO), Utrecht, The Netherlands
[3]Department of Earth Sciences, Royal Holloway University of London (RHUL), Egham, United Kingdom
[4]Environmental Defense Fund (EDF), Utrecht, The Netherlands
[5]Department of Statistics, Colorado State University (CSU), United States of America
[6]Environmental Defense Fund (EDF), Berlin, Germany
[7]Department of Biology, Colorado State University (CSU), United States of America

Correspondence to: Hossein Maazallahi (h.maazallahi@uu.nl)

Abstract. Characterizing and attributing methane (CH_4) emissions across varying scales is important from environmental, safety, and economic perspectives, and is essential for designing and evaluating effective mitigation strategies. Mobile real-time measurements of CH_4 in ambient air offer a fast and effective method to identify and quantify local CH_4 emissions in urban areas. We carried out extensive campaigns to measure CH_4 mole fractions at the street level in Utrecht, The Netherlands (2018 and 2019) and Hamburg, Germany (2018). We detected 145 leak indications (LIs, i.e., CH_4 enhancements of more than 10% above background levels) in Hamburg and 81 LIs in Utrecht. Measurements of the ethane-to-methane ratio (C_2:C_1), methane-to-carbon dioxide ratio (CH_4:CO_2), and CH_4 isotope composition ($\delta^{13}C$ and δD) show that in Hamburg about 1/3 of the LIs, and in Utrecht 2/3 of the LIs (based on a limited set of C_2:C_1 measurements), were of fossil fuel origin. We find that in both cities the largest emission rates in the identified LI distribution are from fossil fuel sources. In Hamburg, the lower emission rates in the identified LI distribution are often associated with biogenic characteristics, or partly combustion. Extrapolation of detected LI rates along the roads driven to the gas distribution pipes in the entire road network yields total emissions from sources that can be quantified in the street-level surveys of 440 ± 70 t yr^{-1} from all sources in Hamburg, and 150 ± 50 t yr^{-1} for Utrecht. In Hamburg, C_2:C_1, CH_4:CO_2, and isotope-based source attributions shows that 50 - 80 % of all emissions originate from the natural gas distribution network, in Utrecht more limited attribution indicates that 70 - 90 % of the emissions are of fossil origin. Our results confirm previous observations that a few large LIs, creating a heavy tail, are responsible for a significant proportion of fossil CH_4 emissions. In Utrecht, 1/3 of total emissions originated from one LI and in Hamburg >1/4 from 2 LIs. The largest leaks were located and fixed quickly by GasNetz Hamburg once the LIs were shared, but 80 % of the (smaller) LIs attributed to the fossil category could not be detected/confirmed as pipeline leaks. This issue requires further investigation.

1 Introduction

Methane (CH_4) is the second most important anthropogenic greenhouse gas (GHG) after carbon dioxide (CO_2) with a global warming potential of 84 compared to CO_2 over a 20-year time horizon (Myhre et al., 2013). The increase of CH_4 mole fraction from about 0.7 parts per million (ppm) or 700 parts per billion (ppb) in pre-industrial times (Etheridge et al., 1998; MacFarling Meure et al., 2006) to almost 1.8 ppm at present (Turner et al., 2019) is responsible for about 0.5 W m^{-2} of the total 2.4 W m^{-2} radiative forcing since 1750 (Etminan et al., 2016; Myhre et al., 2013). In addition to its direct radiative effect, CH_4 plays an important role in tropospheric chemistry and affects the mixing ratio of other atmospheric compounds, including direct and indirect greenhouse gases, via reaction with the hydroxyl radical (OH), the main loss process of CH_4 (Schmidt and

Shindell, 2003). In the stratosphere CH_4 is the main source of water vapor (H_2O) (Noël et al., 2018), which adds another aspect to its radiative forcing. Via these interactions the radiative impact of CH_4 is actually higher than what can be ascribed to its mixing ratio increase alone, and the total radiative forcing ascribed to emissions of CH_4 is estimated to be almost 1 W m^{-2}, ≈ 60 % of that of CO_2 (Fig 8.17 in Myhre et al., 2013). Given this strong radiative effect, and its relatively short atmospheric lifetime of about 9.1 ± 0.9 yr (Prather et al., 2012), CH_4 is an attractive target for short- and medium-term mitigation of global climate change as mitigation will yield rapid reduction in warming rates.

CH_4 emissions originate from a wide variety of natural and anthropogenic sources, for example emissions from natural wetlands, agriculture (e.g. ruminants or rice agriculture), waste decomposition, or emissions (intended and non-intended) from oil and gas activities that are associated with production, transport, processing, distribution, and end-use of fossil fuel sector (Heilig, 1994). Fugitive unintended and operation-related emissions occur across the entire oil and natural gas supply chain. In the past decade, numerous large studies have provided better estimates of the emissions from extended oil and gas production basins (Allen et al., 2013; Karion et al., 2013; Omara et al., 2016; Zavala-Araiza et al., 2015; Lyon et al., 2015), the gathering and processing phase (Mitchell et al., 2015), and transmission and storage (Zimmerle et al., 2015; Lyon et al., 2016) in the United States (US). A recent synthesis concludes that the national emission inventory of the US Environmental Protection Agency (EPA) underestimated supply chain emissions by as much as 60 % (Alvarez et al., 2018). McKain et al. (2015) discussed how inventories may underestimate the total CH_4 emission for cities. Also, an analysis of global isotopic composition data suggests that fossil related emissions may be 60 % higher than what has been previously estimated (Schwietzke et al., 2016). A strong underestimate of fossil fuel related emissions of CH_4 was also implied by analysis of $\delta^{14}C$-CH_4 in pre-industrial air (Hmiel et al., 2020). These emissions do not only have adverse effects on climate, but also represent an economic loss (Xu and Jiang, 2017) and a potential safety hazard (West et al., 2006). While CH_4 is the main component in natural gas distribution networks (NGDNs), composition of natural gas varies from one country or region to another. In Europe the national authorities provide specifications on components of natural gas in the distribution network (Table 8 in UNI MISKOLC and ETE, 2008).

Regarding CH_4 emissions from NGDNs, a number of intensive CH_4 surveys with novel mobile high precision laser-based gas analyzers in US cities have recently revealed the widespread presence of leak indications (LIs: CH_4 enhancements of more than 10 % above background level) with a wide range of magnitudes (Weller et al., 2020; Weller et al., 2018; von Fischer et al., 2017; Chamberlain et al., 2016; Hopkins et al., 2016; Jackson et al., 2014; Phillips et al., 2013). The number and severity of natural gas leaks appears to depend on pipeline material and age, local environmental conditions, pipeline maintenance and replacement programs (von Fischer et al., 2017; Gallagher et al., 2015; Hendrick et al., 2016). For example, NGDNs in older cities with a larger fraction of cast iron or bare steel pipes showed more frequent leaks than NGDNs that use the newer plastic pipes. The data on CH_4 leak indications from distribution systems in cities have provided valuable data for emission reduction in the US cities which allows local distribution companies (LDCs) who are in charge of NGDN to quickly fix leaks and allocate resources efficiently (Weller et al., 2018, von Fischer et al., 2017, Lamb et al., 2016; McKain et al., 2015).

Urban European cities CH_4 emissions are not well known, which requires carrying out extensive campaigns to collect required observation data. Few studies have estimated urban CH_4 fluxes using eddy covariance measurements (Gioli et al., 2012; Helfter et al., 2016), airborne mass balance approaches (O'Shea et al., 2014) and the Radon-222 flux and mixing layer height techniques (Zimnoch et al., 2019). Gioli et al. (2012) showed that about 85 % of methane emissions in Florence, Italy originated from natural gas leaks. Helfter et al. (2016) estimated CH_4 emissions of 72 ± 3 t km^{-2} yr^{-1} in London, UK mainly from sewer sesytem and NGDNs leaks, which is twice as much as reported in the London Atmospheric Emissions Inventory. O'Shea et al. (2014) also showed that CH_4 emissions in greater London is about 3.4 times larger than the report from UK National Atmospheric Emission Inventory. Zimnoch et al. (2019) estimated CH_4 emissions of $(6.2 \pm 0.4) \times 10^6$ m^3 $year^{-1}$ for

Krawko, Poland, based on data for the period of 2005 to 2008 and concluded that leaks from NGDNs are the main emission source in Krawko, based on carbon isotopic signature of CH_4. Chen et al. (2020) also showed that incomplete combustion or loss from temporarily installed natural gas appliances during big festivals can be the major source of CH_4 emissions from such events, while these emissions have not been included in inventory reports for urban emissions.

Here we present the result of mobile in-situ measurements at street level for whole-city surveys in two European cities, Utrecht in the Netherlands (NL) and Hamburg in Germany (DE). In this study, we quantified LIs emissions using an empirical equation from Weller et al. (2019), which was designed based on controlled release experiments from von Fischer et al. (2017), to quantify ground-level emissions locations in urban area such as leaks from NGDN. In addition to finding and categorizing the CH_4 enhancements (in a similar manner as done for the US cities in order to facilitate comparability), we made three additional measurements to better facilitate source attribution: the concomitant emission of ethane (C_2H_6) and CO_2, and the carbon and hydrogen isotopic composition of the CH_4. These tracers allow an empirically based source attribution for LIs. In addition to emission quantifications of LIs across the urban areas in these two cities, we also quantified CH_4 emissions from some of facilities within the municipal boundary of Utrecht and Hamburg using Gaussian plume dispersion model (GPDM).

2 Materials and methods

2.1 Data collection and instrumentation

2.1.1 Mobile measurements for attribution and quantification

Mobile atmospheric measurements at street level were conducted using two Cavity Ring-Down Spectroscopy (CRDS) analyzers (Picarro Inc. model G2301 and G4302) which were installed on the back seat of a 2012 Volkswagen Transporter, (see supplementary information (SI), Sect. S.1.1, Figure S1). The model G2301 instrument provides atmospheric mole fraction measurements of CO_2, CH_4 and H_2O, each of them with an integration time of about 1 s., which results in a data frequency of ≈ 0.3 Hz for each species. The reproducibility for CH_4 measurements was ≈ 1 ppb for 1 s integration time. The G2301 instrument was powered by a 12 V car battery via a DC-to-AC converter. The flow rate was ≈ 187 ml min^{-1}. Given the volume and pressure of the measurement cell (volume = 50 ml and pressure ≈ 190 mbar) the cell is flushed approximately every 3 s, so observed enhancements are considerably smoothed out. The factory settings for CH_4 and CO_2 were used for the water correction.

The G4302 instrument is a mobile analyzer that provides atmospheric mole fraction measurements of C_2H_6, CH_4, and H_2O. The flow rate is 2.2 L min^{-1} and the volume of the cell is 35 ml (operated at 600 mb, thus 21 ml STP) so the cell is flushed in 0.01 s, which means that mixing is insignificant given the 1 s measurement frequency of the G4302. The additional measurement of C_2H_6 is useful for source attribution since natural gas almost always contains a significant fraction of C_2H_6, whereas microbial sources generally do not emit C_2H_6 (Yacovitch et al., 2014). The G4302 runs on a built-in battery which lasts for ≈ 6 h. The instrument can be operated in two modes at ≈ 1 Hz frequency for each species: the CH_4-only mode and the CH_4 - C_2H_6 mode. In the CH_4-only mode the instrument has a reproducibility of ≈10 ppb for CH_4. The factory settings for CH_4 and C_2H_6 were used for the water correction. In the CH_4 - C_2H_6 mode the reproducibility is about 100 ppb for CH_4 and 15 ppb for C_2H_6. For Utrecht surveys (see SI, Sect. S.1.2, Figure S2a), the G4302 was not yet available for the initial surveys in 2018, but it was added for the later re-visits (see SI, Sect. S.1.2, Table S1). For Hamburg (see SI, Sect. S.1.2, Figure S2b), both instruments operated during the entire intensive 3-week measurement campaign in Oct/Nov 2018 (see SI, Sect. S.1.2, Table S2). The time delay from the inlet to the instruments was measured and accounted for in the data processing procedure. The Coordinated Universal Time (UTC) time shifts between the Global Positioning System (GPS) and the two Picarro instruments

were corrected for each instrument in addition to the inlet delay (see SI, Sect. S.1.2, Table S1 and Table S2). The clocks on the Picarro instruments were set to UTC but showed drift over the period of the campaigns. We recorded the drifts for each day's survey and corrected to UTC time. The data were also corrected for the delay between air at the inlet and the signal in the CH_4 analyzers. This delay was determined by exposing the inlet to three small CH_4 pulses from exhaled breath, ranging from 5-30 seconds, depending on the instrument and tubing length. We averaged the three attempts to determine the delay for each instrument and used the delays for each instrument. Individual attempts were 1 to 2 s different from each other. For the G4302 the delay was generally about 5 s and for the G2301 it was about 30 s; the difference is mainly due to the different flow rates. The recorded CH_4 mole fractions were projected back along the driving track according to this delay.

One-quarter inch Teflon tubing was used to pull in air either from the front bumper (0.5 m above ground level) to the G2301 or from the rooftop (2 m above ground level) to the G4302. To avoid dust into the inlets for both instruments, Acrodisc® syringe filter, 0.2 μm was used for G2301 and Parker Balston 9933-05-DQ was used for G4302. The G2301 was used for quantification and attribution purposes and the G4302 mainly for attribution. After data quality check, a comparison between the two instruments during simultaneous measurements showed that all LIs were detectable by both instruments despite difference in inlet height (see SI, Sect. S.1.3, Figure S3). A comparison between the two instruments during simultaneous measurements showed that all LIs were detected by both instruments despite difference in instrument characteristics and inlet height. In the majority of cases CH_4 enhancements for each LI from both instruments were similar to each other. We note that there is likely a compensation of differences from two opposing effects between the two measurement systems. The inlet of the G2301 was at the bumper, thus closer to the surface sources, but the rather low flow rate and measurement rate of the instrument lead to some smoothing of the signal in the cavity. Because of the high gas flow rate, signal smoothing is much reduced for the G4302, but the inlet was on top of the car, thus further away from the surface sources (see Table S3 in SI, Sect. S.1.3). The vehicle locations were registered using a GPS system that recorded the precise driving track during each survey.

2.1.2 Target cities: Utrecht and Hamburg

Utrecht is the 4th largest city in the Netherlands with population of approximately 0.35 million inhabitants within an area of roughly 100 km^2. It is located close to the center of the Netherlands and is an important infrastructural hub in the country. The Utrecht city area that we target in this study is well constrained by a ring of highways around the city (A27, A12, A2, and N230) with inhabitants of approximately 0.28 million living within this ring on roughly 45 km^2 of land. Figure S2a (see SI, Sect. S.1.2) shows the streets that were driven in Utrecht and Figure 1a shows the street coverage over four street categories (level 1, 2, 3, residential, and unclassified) obtained from the Open Street Map (OSM; www.openstreetmap.org). Table S4 (see SI, Sect. S.1.5) provides information on road coverage based on different street categories. The hierarchy of OSM road classes is based on the importance of roads in connecting parts of the national infrastructure. Level 1 roads are primarily larger roads connecting cities, level 2 roads are the second most important roads and part of a greater network to connect smaller towns, level 3 roads have tertiary importance level and connect smaller settlements and districts. Residential roads are roads which connect houses and unclassified roads have the lowest importance of interconnecting infrastructure. Moreover, several transects were also made to measure the atmospheric mole fraction of CH_4 from the road next to the waste water treatment plant (WWTP) in Utrecht – a potentially larger single source of CH_4 emissions in the city (see SI, Sect. S.1.6, Table S5).

Hamburg is the 2nd largest city in Germany (about 1.9 million inhabitants, 760 km^2 area) and hosts one of the largest harbors in Europe. The study area in Hamburg is North of the Elbe river (Figure 1b) with ≈1.4 million inhabitants on about 400 km^2 land. Figure S2b (see SI, Sect. S.1.2) shows the streets that were covered in Hamburg and Figure 1b shows the street coverage categorized in the four categories of OSM. More information on road coverage based on OSM street categories are provided in Table S4 (see SI, Sect. S.1.5). The local distribution companies (LDCs) in Utrecht (STEDIN

(https://www.stedin.net/)) and Hamburg (GasNetz Hamburg (https://www.gasnetz-hamburg.de)) confirmed that full pipeline coverages are available beneath all streets. Therefore, the length of roads in the study area of Utrecht and Hamburg are representatives of NGDNs length. The Hamburg harbor area hosts several large industrial facilities that are related to the midstream / downstream oil and gas sector including refineries and storage tanks. An oil production site (oil well, separator and storage tanks) at Allermöhe (in Hamburg-Bergedorf) was also visited. Information from the State Authority for Mining, Energy and Geology (LBEG, 2018) was used to locate facilities. Precise locations of the facilities surveyed are given in the Table S6 (see SI, Sect. S.1.6). In order to separate these industrial activities from the NGDNs emissions in this study, CH_4 emissions from these locations were estimated, but evaluated apart from the emissions found in each city. The reported in-situ measurement, GPS data, and boundary of study areas reported here are available on the Integrated Carbon Observation System (ICOS) portal (Maazallahi et al., 2020b).

2.1.3 Driving strategy

The start/end point for each day's measurement surveys across Utrecht and Hamburg were the Institute for Marine and Atmospheric research Utrecht (IMAU; Utrecht University) and the Meteorological Institute (MI; Hamburg University), respectively. From these starting locations, each day's surveys targeted the different districts and neighborhoods of the cities (see SI, Sect. S.1.2, Table S1 and Table S2). Measurement time periods and survey areas were chosen to select favorable traffic and weather conditions and to avoid large events (e.g., construction; see SI, Sect. S.1.5, Figure S4), which normally took place between 10 - 18 LT. Average driving speeds on city streets were in the range of 17 ± 7 km h^{-1} in Utrecht and 20 ± 6 km h^{-1} in Hamburg.

As part of our driving strategy, we revisited locations where we had observed enhanced CH_4 readings (see SI, Sect. S.1.7, Figure S5). Not all recorded CH_4 mole fraction enhancements are necessarily the result of a stationary CH_4 source. For example, they could be related to emissions from vehicles which run on compressed natural gas, or vehicles operated with traditional fuels but with faulty catalytic converter systems. Later we will discuss how to exclude or categorize these unintended signals (see Sect. 2.2.2 and Sect. 2.3.1). Therefore, we revisited a large number of locations (65 in Utrecht (≈80 %) and 100 in Hamburg (≈70 %)) where enhanced CH_4 had been observed in during the first survey in order to confirm the LIs. In contrast to the measurements carried out in many cities in the United States (US) (von Fischer et al., 2017), our measurements were not carried out using Google Street View cars, but with a vehicle from the Institute for Marine and Atmospheric research Utrecht (IMAU), Utrecht University (see SI, Sect. S.1.1, Figure S1). Due to time and budget restrictions, it was not possible to cover each street at least twice, as done for the US cities. After evaluation of the untargeted first surveys that covered each street at least once, targeted surveys were carried out for verification of observed LIs and for collection of air samples at locations with high CH_4 enhancements. The rationale behind this measurement strategy is that if an enhancement was not recorded during the first survey, it obviously cannot be verified in the second survey. The implications of the difference in the measurement strategy will be discussed in the Results and Discussion sections below.

In total, approximately 1,300 km of roads were driven during Utrecht surveys and about 2,500 km during the Hamburg campaign. In Utrecht, some re-visits were carried out several months to a year after the initial surveys in order to check on the persistence of the LIs. In Hamburg, revisits were also performed within the 4-week intensive measurement period. Further details about the driving logistics are provided in the SI (Sect. S.1.6, Table S1 and Table S2). It is possible that pipeline leaks that were detected during the initial survey were repaired before the revisit, and the chance of this occurring increases as the time interval between visits gets longer.

2.1.4 Air sample collection for attribution

In addition to the mobile measurement of C_2H_6 and CO_2 for LIs attributions purposes, samples for lab isotope analysis of $\delta^{13}C$-CH_4 and $\delta^{2}H$-CH_4 (hereinafter $\delta^{13}C$ and δD respectively) were collected during the revisits at locations that had displayed high CH_4 enhancements during the first surveys. Depending on the accessibility and traffic, samples were either taken inside the car (see SI, Sect. S.1.8, Figure S6a) using a tubing from the bumper inlet, or outside the car on foot using the readings from the G4302 to find the best location within the plume (see SI, Sect. S.1.8, Figure S6b). All the samples taken in the North Elbe study area and from most of the facilities were collected when the car was parked, but the samples inside the New Elbe tunnel and close to some facilities where there was no possibility to park were taken in motion while we were within the plume. The sampling locations across the North Elbe study area of Hamburg were determined based the untargeted surveys, and the confirmation during revisits. The C_2H_6 information was not used in the selection of sampling locations in order to avoid biased sampling. Sampling locations from the facilities were determined based on wind direction, traffic, and types of different activities. Samples for isotope analysis were collected in non-transparent aluminum-coated Tedlar Supelco, Seupel™ Inert SCV Gas Sampling Bag (2 L) and SKC, Standard FlexFoil® Air Sample Bags (3 L) using a 12 V pump and 1/4-inch Teflon tubing which pumps air with flow rate of ≈0.25 L min^{-1}. In total, 103 bag samples were collected at 24 locations in Hamburg, 14 of them in the city area North of the Elbe river and 10 at larger facilities. Usually, three individual samples were collected at each source location, plus several background air samples on each sampling day. This sampling scheme generally results in a range of mole fractions that allow source identification using a Keeling plot analysis (Keeling, 1958, 1961). Fossil CH_4 sources in the study areas of this paper (inside the ring for Utrecht and north Elbe in Hamburg) refers to emissions originating from natural gas leaks.

2.1.5 Meteorological Data

Meteorological information reflecting the large scale wind conditions during the campaigns were obtained from measurements at the Cabauw tower (51.970263° N, 4.926267° E) operated by Koninklijk Nederlands Meteorologisch Instituut (KNMI) (Van Ulden and Wieringa, 1996) for Utrecht and Billwerder tower (53.5192° N, 10.1029° E) operated by the MI at Hamburg University (Brümmer et al., 2012) for Hamburg. The wind direction and wind speed data from the masts were used for planning the surveys. Pressure and temperature measurements were used to convert volume to mass fluxes for CH_4. We also used information from the towers for the GPDM calculations of the emission rates from larger facilities, because the local wind measurements from the 2-D anemometer were not logged continuously due to failure in logging setup of the measurements. In Utrecht, the Cabauw tower is located about 20 km from the WWTP. In Hamburg Billwerder tower is about 18 km from the Soil and Compost company and about 8 km from oil production facilities. Uncertainties over the wind data will be described later.

2.2 Emission quantification

2.2.1 Data preparation and background extraction of mobile measurements

The first step of the evaluation procedure is quality control of the data from both CH_4 analyzers and the GPS records. Periods of instrument malfunction and unintended signals based on notes written during each day's measurements were removed from the raw data. Extraction of the LIs from in-situ measurements requires estimation of the background levels (see SI, Sect. S.2.1, Figure S7). We estimated CH_4 background as the median value of ± 2.5 min of measurements around each individual point as suggested in Weller et al. (2019). For estimating the CO_2 background level we used the 5^{th} percentile of ± 2.5 min of measurements around each individual point (Brantley et al., 2014; Bukowiecki et al., 2002). The background determination method for CH_4 was selected from Weller et al. (2019) to follow the emission quantification algorithm for the

urban studies, and while this algorithm doesn't include background extraction for CO_2, we chose commonly adopted method of background determination for this component. These background signals were subtracted from the measurement time series to calculate the CH_4 and CO_2 enhancements. For C_2H_6, the background was considered zero as it is normally present at a very low mole fraction; between ~0.4-2.5 ppb (Helmig et al., 2016), and is lower than the G4302 detection limit.

2.2.2 Quantification of methane emissions from leak indications

We wrote an automated MATLAB® script (available on GitHub from Maazallahi et al. (2020a)) based on the approach initially introduced in von Fischer et al. (2017), and improved in Weller et al. (2019). This algorithm was designed to quantify CH_4 emissions from ground-level emission release locations within 5-40 m from the measurement (von Fischer et al., 2017), such as pipeline leaks and has been demonstrated that the algorithm adequately estimates the majority of those emissions from a city (Weller et al., 2018). Using the same algorithm also ensures that results are comparable between European and US cities. The individual steps will be described below. Mapping and spatial analysis were conducted using Google Earth and ESRI ArcMap software. A flow diagram of the evaluation procedure is provided in the SI (Sect. S.2.2, Figure S8).

Following the algorithm from von Fischer et al. (2017), measurements at speeds above 70 km h^{-1} were excluded, as the data from the controlled release experiments (von Fischer et al., 2017) were not reliable at high speed (Weller et al., 2019). We also excluded measurements during periods of zero speed (stationary vehicle) to avoid unintended signals coming from other cars running on compressed natural gas when the measurement car was stopped in traffic. In order to merge the sharp 1 Hz-frequency records of the GPS with the ≈ 0.3 Hz data from the G2301 analyzer, the CH_4 mole fractions were linearly interpolated to the GPS times.

Weller et al., (2019) established an empirical equation to convert LIs observed with a Picarro G2301 in a moving vehicle in urban environments into emission rates based on a large number of controlled release experiments in various environments (Eq. (1)).

$$\mathrm{Ln}(C) = -0.988 + 0.817 * \mathrm{Ln}(Q) \quad (1)$$

In this equation, C represents CH_4 enhancements above the background in ppm and Q is the emission rate in L min^{-1}. Weller et al., (2019) used controlled releases to demonstrate that the magnitude of the observed methane enhancement is related to the emission rate and carefully characterized the limitations and associated errors of this equation. We used Eq. (1) to convert CH_4 enhancements encountered during our measurements in Utrecht and Hamburg to emission rates, and we use these estimates to categorize LIs into three classes: high (emission rate > 40 L min^{-1}), medium (emission rate 6− 40 L min^{-1}) and low (emission rate 0.5 - 6 L min^{-1}), following the categories from von Fischer et al. (2017) (Table 1).

The spatial extent of individual LIs was estimated as the distance between the location where the CH_4 mole fraction exceeded the background by more than 10 % (≈ 0.200 ppm; as used in von Fischer et al. (2017) and Weller et al. (2019)) to the location where it fell below this threshold level again. LIs which stay above the threshold for more than 160 m were excluded in the automated evaluation because we suspect that such extended enhancements are most likely not related to leaks from the NGDN (von Fischer et al., 2017).

In a continuous measurement survey on a single day, consecutive CH_4 enhancements above background observed within 5 seconds were aggregated and the location of the emission source was estimated based on the weighted averaging of coordinates (Eq. (2)). Decimal degree coordinates were converted to Cartesian coordinates (see SI, Sect. S.2.3, Figure S9) relative to local references (see SI, Sect. S.2.3, Table S7). In Utrecht, the Cathedral tower (Domtoren) and in Hamburg the St. Nicholas' Church were selected as local geographic datums. LIs observed on different days at similar locations were clustered and interpreted as one point source when circles of 30 m radius around the centre locations overlapped, similar to Weller et al., (2019). The enhancement of the cluster was assigned the maximum observed mole fraction and located as the weighted

average of the geographical coordinates of the LIs within that cluster (Eq. (2) from Weller et al. (2019)), where w_i is CH_4 enhancement of each LI.

$$(\text{lon, lat}) = \frac{\sum_{i=1}^{n} w_i * (lon_i, lat_i)}{\sum_{i=1}^{n} w_i} \quad (2)$$

We compared the outputs of our software to the one developed by Colorado State University (CSU) for the surveys in US cities (von Fischer et al., 2017; Weller et al., 2019). 30 LIs were detected and no significant differences were observed (linear fit equation y = 1.00 * x - 0.00, $R^2 = 0.99$) (see SI, Sect. S.2.4, Figure S10). As mentioned above, in our campaign-type studies not all streets were visited twice, so this criterion was dropped from the CSU algorithm. Instead, we used explicit source attribution by co-emitted tracers.

The emission rate per km of road covered during our measurements was then scaled up to the city scale using the ratio of total road length within the study area boundaries derived from OSM to the length of streets covered, and converted to a per-capita emission using the population in the study areas based on LandScan data (Bright et al., 2000). Note that in this up-scaling practice, emission quantified from facilities were excluded.

To account for the emission uncertainty, similar to Weller et al. (2018) for the US city studies, we used a bootstrap technique which was initially introduced in Efron (1979, 1982), as this technique is adequate in resampling of both parametric and non-parametric problems with even non-normal distribution of observed data. Tong et al. (2012) indicated that bootstrap resampling technique is sufficiently capable in estimating uncertainty of emissions with sample size of equal or larger than 9. Efron and Tibshirani (1993) suggested that minimum of 1,000 iterations are adequate in bootstrap technique. In this study, we used non-parametric bootstrap technique to account for the uncertainty of total CH_4 emissions from all LIs in each city with 30,000 replications. As mentioned above the algorithm is based on CH_4 enhancements of measurement with 5-40 m distance from controlled release location, and can produce large uncertainty for emission quantification of individual LI (Figure 4 in Weller et al. (2019)), but with sufficient number of sample size, the uncertainty associated with total emission quantified in an urban area is more precise.

2.2.3 Quantification of methane emissions from larger facilities

Apart from the natural gas distribution network, there are larger facilities in both cities that are potential CH_4 sources within the study area. Several facilities in or around the cities were visited during the mobile surveys to provide emission estimates. We applied a standard point source GPDM (Turner, 1969) to quantify methane emissions from these larger facilities. A flowchart describing the steps taken during quantification from facilities in given in SI (Sect. S.2.5., Figure S11). We note that emission quantification using GPDM with data from mobile measurements is prone to large errors (factor of 3 or more) (Yacovitch et al., 2018) especially when the measurements are carried out close to the source. In this study, we also report the data obtained from larger facilities, since rough emission estimates from facilities can be obtained in the city surveys. Caulton et al. (2018) discuss uncertainties of emission quantification with GPDM. Individual facilities were visited during the routine screening measurements and during revisits for LI confirmation and air sampling.

In Utrecht, the WWTP is located in the study area and streets around this facility were passed several times during surveys. In Hamburg, we initially performed screening measurements in the harbor area (extensive industrial activities) and near an oil production site and then revisited these sites for further quantification and isotopic characterization. The data from the oil production site can be fit reasonably well with a GPDM and were therefore selected for quantification, similar to studies in a shale gas production basin in the USA (Yacovitch et al., 2015) and in the Netherlands (Yacovitch et al., 2018).

$$C(x,y,z) = \frac{Q}{2*\pi*u*\sigma_y*\sigma_z} * \{ \exp\left(\frac{-(z-z_{source})^2}{2*\sigma_z^2}\right) + \exp\left(\frac{-(z+z_{source})^2}{2*\sigma_z^2}\right)\} * \exp\left(\frac{-y^2}{2*\sigma_y^2}\right)\} \quad (3)$$

In Eq. (3), C is the CH_4 enhancement converted to the unit of g/m^3 at cartesian coordinates x, y, and z relative to the source ($[x\ y\ z]_{source} = 0$), x is the distance of the plume from the source aligned with the wind direction, y is the horizontal axis

perpendicular to the wind direction, z is the vertical axis. Q is emission rate in g s^{-1}, u (m s^{-1}) is the wind speed along the x-axis, and σ_y and σ_z are the horizontal and vertical plume dispersion parameters (described below), respectively.

Determination of an effective release location is a challenge for the larger facilities. Effective emission locations for each facility were estimated based on wind direction measurements and the locations of maximum CH_4 enhancements. The facilities were generally visited multiple times under different wind conditions. The locations of the maximum CH_4 enhancements were then projected against the ambient wind, and the intersection point of these projections during different wind conditions was defined as effective emission location of the facility. At least two measurement transects with different wind direction were used to estimate the effective location of the source. If wind directions, road accessibility or the shape of plumes were not sufficient to indicate the effective source location, the geographical coordinates of centroids of the possible sources using Google Earth imageries and field observations were used to determine the effective emission location. For the WWTP in Utrecht we also contacted the operator and asked for the location of sludge treatment as it is the major source of CH_4 emissions (Paredes et al., 2019; Schaum et al., 2015).

Neumann and Halbritter (1980) showed that the main parameters in sensitivity analysis of GPDM are the wind speed and source emission height in close distance and the influence of emission height become less further downwind compared to the mixing layer height. In this study, the heights of emission sources were low (<10m) and estimated during surveys and/or using Google Earth imageries, and considering that such a larger measurement distance from the facilities, the main sources of uncertainty of the emission estimates for the WWTP and Compost and Soil company are most likely the mean wind speed and for the upstream facilities in Hamburg the major sources of uncertainties can be the mean wind speed and emission height. We considered 0-4 m source height for the WWTP in Utrecht, and for the upstream facilities in Hamburg we considered 0-5 m emission height for the Compost and Soil site, 0-2 m for the separator, 0-10 m for the storage tank, and 0-1 m for the oil extraction well-head. We used 1 m interval for each of these height ranges to quantify emissions in GPDM.

Cross wind horizontal dispersions σ_y were estimated from the measured plumes by fitting a Gaussian curve to the individual plumes from each set during each day's survey. A set of plumes is defined as a back to back transects during a period of time downwind each facility on different days. Later average emissions from all sets of plumes were used to report CH_4 emission for each of the facilities. A suitable Pasquill–Gifford stability class was then determined by selecting a pair of parameters (Table 1-1 in EPA, 1995) that matches best and give the closest number to the with the fitted value of σ_y. Vertical dispersions σ_z were then estimated using the identified Pasquill–Gifford stability class in the first step, using the distances to the source locations (Table 1-2 in EPA, 1995). Uncertainties due to these estimates will be discussed below. Mass emission rates were calculated using the metric volume of CH_4 at 1 bar of atmospheric pressure (0.715 kg m^{-3} at 0 °C and 0.666 kg m^{-3} at 20 °C, P. 1.124 in IPCC, 1996), and linear interpolation was used for temperatures in between.

Due to technical issues, local wind data were not logged continuously and thus we used wind data from two towers which are 8 to 20 km away from the facilities we focused for emission quantifications. These distances introduce extra uncertainties in analyzing the emissions using GPDM mainly on the wind speed. By comparing some of the local high-quality wind data to data from the towers, we estimated that the local wind speed is within the range of ± 30 % of the collected tower data. This range was adopted to estimate the wind speed for emission quantifications for the set of plumes measured downwind of the facilities. The wind directions were aligned at local scale of each facility based on the locations of sources and locations of maxima of average CH_4 enhancements from a set of transects in each day's survey and we considered ± 5° uncertainty in wind direction for the GPDM quantification.

2.3 Emission attribution

2.3.1 Mobile C_2H_6 and CO_2 measurements

During the Utrecht campaign, the overall mole fraction of CH_4 and C_2H_6 in the NGDN was ≈ 80 % and ≈ 3.9 % (STEDIN, personal communication) and in Hamburg the mole fraction of CH_4 and C_2H_6 in the NGDN was about ≈ 95 % and ≈ 3.4 % (GasNetz Hamburg, personal communication) respectively. This ratio can vary depending on the mixture of gas compositions from different suppliers, but should meet the standards on the gas compositions in the Netherlands (65 – 96 mol-% for CH_4 and 0.2 – 11 mol-% for C_2H_6 (ACM, 2018)) and in Germany (83.64 – 96.96 mol-% for CH_4 and 1.06 – 6.93 mol-% for C_2H_6 (DVGW, 2013)). Compressed natural gas vehicles can be mobile CH_4 emission sources (E. K. Nam et al., 2004; Curran et al., 2014; Naus et al., 2018; Popa et al., 2014) and in this study we also observed CH_4 signals from vehicles. For example, the point to point C_2H_6:CH_4 ratio (C_2:C_1) calculated from road measurements of a car exhaust shown in Figure S12 (see SI, Sect. S.2.6) is 14.2 ± 7.1 %. During the campaigns in Utrecht and Hamburg the C_2:C_1 of NGDNs was less than 10 % and in our study, we removed all the locations where the C_2:C_1 ratio was greater than 10 %. CH_4 emissions from combustion processes are always accompanied by large emissions of CO_2 and can therefore be identified based on the low CH_4:CO_2 emission ratio. In this study, LIs with CH_4:CO_2 ratio between 0.02 and 20 with R^2 greater than 0.8 were attributed to combustion.

2.3.2 Lab isotopic analysis of $\delta^{13}C$ and δD

After sample collections, the bag samples were returned to the IMAU for analysis of both $\delta^{13}C$ and δD (Brass and Röckmann, 2010) and some samples were analyzed at the Greenhouse Gas Laboratory (GGL) in the department of Earth Sciences, Royal Holloway University of London (RHUL) for $\delta^{13}C$ (Fisher et al., 2006) (see SI, Sect. S.2.7, Figure S13).

At the IMAU, we used isotope ratio mass spectrometry (IRMS) instrument of ThermoFinnigan MAT DeltaPlus XL (Thermo Fisher Scientific Inc., Germany). We used a reference cylinder calibrated against Vienna Pee Dee Belmnite (V-PDB) for $\delta^{13}C$ and Vienna Standard Mean Ocean Water (V-SMOW) for δD at the at the Max Planck Institute for Biogeochemistry (MPI-BGC), Jena, Germany (Sperlich et al., 2016). The cylinder contained CH_4 mole fraction of 1975.5 ± 6.3 ppb, $\delta^{13}C$ = -48.14 ± 0.07 ‰ vs V-PDB and δD = -90.81 ± 2.7 ‰ vs V-SMOW. The samples were pumped through a magnesium perchlorate ($Mg(ClO_4)_2$) dryer before the CH_4 extraction steps. Each sample was measured at least 2 times (up to four times) for each isotope. Every other sample, the reference gas was also measured 3 times for $\delta^{13}C$ and δD. Each measurement, from the CH_4 extraction to the mass spectrometer, took ≈ 30 minutes.

At the GGL, Flex foil SKC bag samples were each analyzed for methane mole fractions and $\delta^{13}C$. Methane mole fractions were determined using a Picarro G1301 CRDS, which measured every 5 seconds for 2 minutes resulting in a precision ± 0.3 ppb (Lowry et al., 2020; France et al., 2016; Zazzeri et al., 2015). Each sample was then measured for stable isotopes ($\delta^{13}C$-CH_4) using an Elementar Trace gas and continuous-flow gas chromatography isotope ratio mass spectrometry (CF-GC-IRMS) system (Fisher et al., 2006), which has an average repeatability of ± 0.05 ‰. CH_4 extraction was preceded by drying process using $Mg(ClO_4)_2$. Each sample was measured 3 times for $\delta^{13}C$-CH_4, where the duration of each analysis was ≈ 20 minutes. Both instruments are calibrated weekly to the WMO X2004A methane scale using air filled cylinders that were measured by the National Oceanic and Atmospheric Administration (NOAA), and cylinders that were calibrated against the NOAA scale by the MPI-BGC (France et al., 2016; Lowry et al., 2020).

The analytical systems for isotope analysis have been described, used and/or compared in several previous publications (Fisher et al., 2011; Röckmann et al., 2016; Umezawa et al., 2018; Zazzeri et al., 2015). Measurement uncertainties in $\delta^{13}C$ and δD are 0.05-0.1 ‰ and 2-5 ‰ respectively.

After the LIs were analyzed and quantified, the measurements of C_2H_6, CO_2, and isotopic composition from the air samples were used for source attribution. We characterize the observed LIs as of fossil origin when they had a concomitant C_2H_6 signal between 1 % and 10 % of the CH_4 enhancements and when the isotopic composition was in the range -50 to -40 ‰ for $\delta^{13}C$ and -150 to -200 ‰ for δD. A LI was characterized as microbial when there was no C_2H_6 signal (<1 % of the CH_4 enhancements larger than 500 ppb), $\delta^{13}C$ was between -55 ‰ and -70 ‰ and δD was between -260 and -360 ‰ (Figure 7 in Röckmann et al., 2016). LIs with enhancements of CH_4 lower than 500 ppb and no C_2H_6 signals were categorized as unclassified. LIs with no C_2H_6 signals, no significant CH_4:CO_2 ratio, and no information on $\delta^{13}C$ and δD were also categorized as unclassified. The source signatures for each sampling location were determined by a Keeling plot analysis of the three samples collected in the plumes and a background sample taken on the same day.

3 Results

3.1 Quantification of CH_4 emissions across Utrecht and Hamburg

Table 2 summarizes the main results from the surveys in Hamburg and Utrecht. The amount of km of roads covered in Hamburg is roughly a factor of 2 larger than in Utrecht, and also the number of detected LIs is roughly a factor of 2 larger, for all three categories. This shows that the overall density of LIs (km covered per LI) in both cities is not very different. Specifically, a LI is observed every 5.6 km in Utrecht and every 8.4 km in Hamburg. While not all streets were visited twice in both cities (see SI, Sect. S.1.5, Table S4) 80 % of LIs in Utrecht and 69 % of LIs in Hamburg were revisited which account for 91 % and 86 % of emissions respectively in the study areas. During revisits, 60 % of CH_4 emissions in Utrecht and 46 % of emissions in Hamburg were confirmed. In both cities, all LIs in the high emission category were re-observed. In some cases, re-visits were carried out several months after first detection, and the LIs were still confirmed (e.g. see SI, Sect. S.1.7, Figure S5).

The distribution of CH_4 LIs across the cities of Utrecht and Hamburg is shown in Figure 2. As shown in Table 2, a total of 145 significant LIs were detected in Hamburg and 81 in Utrecht; these LIs cover all three LI categories. Two LIs in Hamburg and one LI in Utrecht fall in the high (red) emission category; the highest LI detected in Utrecht and Hamburg corresponded to emission rates of ≈ 100 L min^{-1} and ≈ 70 L min^{-1}, respectively. Noted that estimates for individual leaks with the Weller et al. (2019) algorithm can have large error, thus these results are indicative of large leaks, but the precise emission strength is very uncertain. Six LIs in Utrecht and 16 LIs in Hamburg fall in the middle (orange) emission category, and 127 LIs in Hamburg and 74 LIs in Utrecht fall in the low (yellow) emission category. The distribution of emissions over the three categories is also similar between the two cities, with roughly one third of the emissions originating from each category (Figure 2), but the number of LIs in each category is different. The contribution of LIs in the high emission category is about a third of the total observed emissions (35 % in Utrecht is (1 LI) and in 30 % in Hamburg (2 LIs)).

CH_4 emitting locations were categorized based on the roads where the LIs were observed (Figure 1, Figure 2, Figure 3, and Table S8 in SI, Sect. S.3.1). Average emission rates per LI as derived from equation (1) are similar for the two cities with 3.6 L min^{-1} LI^{-1} in Utrecht and 3.4 L min^{-1} LI^{-1} in Hamburg, but they are distributed differently across the road (Figure 1). In Utrecht, emitting locations on level 2 roads contributed the most (50 % of emissions) to the total emissions while in Hamburg the majority of the emissions occurred on residential roads (56 % of total emissions). This shows that the major leak indications may happen on different road classes in different cities and there is no general relation to the size of streets between these two cities.

In Figure 4, we compare cumulative CH_4 emissions for Utrecht and Hamburg to numerous US cities (Weller et al., 2019). After ranking the LIs from largest to smallest, it becomes evident that the largest 5 % of the LIs account for about 60 % of emissions in Utrecht, and 50 % of the emissions in Hamburg.

As mentioned above, the observed total emission rates observed on roads in urban environment in the two cities are relatively similar when normalized by the total amount of km covered, 0.64 L min^{-1} km^{-1} for Utrecht and 0.4 L min^{-1} km^{-1} for Hamburg (Table 2). Using these two emission factors, the observed emission rates (≈110 t yr^{-1} in Utrecht and ≈180 t yr^{-1} in Hamburg) were up-scaled to the entire road network in the two cities, ≈ 650 km in Utrecht and ≈ 3,000 km in Hamburg. This includes the implicit assumption that the pipeline network is similar to the street network. Total up-scaled emission rates based on mobile measurements on roads in urban environment before considering attribution analysis over LI locations are 150 t yr^{-1} and 440 t yr^{-1} across the study areas of Utrecht and Hamburg respectively. Distributing the calculated emission rates over the population in the city areas yields emission rates of 0.54 ± 0.15 kg yr^{-1} $capita^{-1}$ for Utrecht and 0.31 ± 0.04 kg yr^{-1} $capita^{-1}$ for Hamburg (see SI, Sect. S.3.2, Figure S14).

3.2 Attribution of CH_4 emissions across Utrecht and Hamburg

Figure 5 shows the results of the isotope analysis for the 21 locations in Hamburg where acceptable Keeling plots were obtained (see SI, Sect. S.3.3, Table S9 and Table S10). The results cluster mostly in three groups, which are characterized by the expected isotope signatures for fossil, microbial, and pyrogenic samples as described in Röckmann et al., (2016).

Average isotope signatures for the LIs in the city of Hamburg were $\delta^{13}C$ = -52.3 ± 5.1 ‰ and δD = -298.4 ± 30.3 ‰ for the samples characterized as microbial and $\delta^{13}C$ = -41.9 ± 1.0 ‰ and δD = -196.1 ± 10.6 ‰ for the samples characterized as fossil (Figure 5). One sample from the Hamburg city area displays a very high source signature of $\delta^{13}C$ = -23 ‰ and δD = -153 ‰. The origin of CH_4 with such an unusual isotopic signature could not be identified and it is considered an outlier. In Hamburg, 10 % of the LI locations (38 % of emissions) on the north side of Elbe were sampled for isotope analysis. The lab isotopic attributions show that the LIs with the higher emission rates are mostly caused by emission of fossil CH_4. 79 % of the inferred emissions at 38 % of the LIs were identified as of fossil origin, 20 % of emissions at 54 % of the LIs as of microbial origin (for an identified source see SI, Sect. S.3.3, Figure S15), 1 % of emissions at 8 % of LIs as of pyrogenic origin.

In Hamburg, during three passes through the new Elbe tunnel (see SI, Sect. S.3.4, Figure S16) a CH_4:CO_2 of 0.2 ± 0.1 ppb:ppm was derived for combustion-related emission. During the surveys of open roads, clear CH_4:CO_2 correlations were observed for several LIs and an example of a measurement of car exhaust is shown in Figure S12a (see SI, Sect. S.2.6) with CH_4:CO_2 = 1.6 ppb:ppm. Previous studies have shown relatively low CH_4:CO_2 ratios of $4.6*10^{-2}$ ppb:ppm (Popa et al., 2014), 0.41 ppb ppm^{-1} (E. K. Nam et al., 2004), and 0.3 ppb:ppm (Naus et al., 2018) when cars work under normal conditions. During cold engine (Naus et al., 2018) or incomplete combustion conditions, the fuel to air ratio is too high, which results in enhanced emission of black carbon particles and reduced carbon compounds, so higher CH_4:CO_2 ratios. Hu et al. (2018) reported 2 ± 2.1 ppb:ppm in a tunnel, but 12 ± 5.3 ppb:ppm [1] on roads. In addition to car exhaust, there are other combustion sources which can affect CH_4 and CO_2 mole fractions at the street level including natural gas water heater (CH_4:CO_2 ratio of ≈ 2 ppb:ppm; Lebel et al., 2020), restaurant kitchens, etc. Based on the CH_4:CO_2 ratio (ppb:ppm) criterion defined above (see Sect. 2.3.1), 17 % of LIs (10 % of emissions) can be attributed to combustion (see SI, Sect. S.3.4, Figure S17) with a mean CH_4:CO_2 ratio of 3.2 ± 3.9 ppb:ppm (max = 18.7 and min = 0.8 ppb:ppm). The C_2:C_1 ratio for these LIs attributed to combustion in Hamburg was 7.8 ± 3.5 %. In Utrecht 7 % of LIs (2 % of emissions) are attributed to combustion with a mean CH_4:CO_2 ratio of 9.8 ± 5.8 ppb:ppm (max = 16.7 and min = 3.0 ppb:ppm).

Based on the C_2H_6 signals, 64 % of the emissions (33 % of LIs) were characterized as fossil, while 25 % of emissions (20 % of LIs) were identified as microbial. Due to low CH_4 and C_2H_6 enhancements, 47 % of the locations (11 % of emission) were considered unclassified. The C2:C1 ratio for the LIs attributed to emissions from NGDNs in Hamburg study area (North Elbe) is 4.1 ± 2.0 %. The oil production site in south-east Hamburg had a higher C_2:C_1 ratio of 7.1 ± 1.5 %.

In Utrecht, C_2H_6 was measured only during four surveys in February, April, and June 2019 (revisits of 2-day surveys across the city center and 2 days to LIs with high emission rates) as the CH_4 - C_2H_6 analyzer was not available during the first

campaign. The C_2:C_1 ratios from this limited survey indicates that 93 % of emissions (69 % of the LIs across the city centre, including combustions) are likely from fossil sources (Table 2) and 73 % of emissions (43 % of the LIs, including combustion) out of all LIs. In Utrecht, the C_2:C_1 ratio for the LIs attributed to NGDNs is 3.9 ± 0.8 %.

3.3 Quantification of CH_4 plume from larger facilities

Table 3 shows the emission rate estimates from the larger facilities in Utrecht and Hamburg. CH_4 plumes from the WWTP (Figure 6 and in SI, Sect. S.1.6., Table S5) were intercepted numerous times during the city transects, and the error estimate in Table 3 represents one standard deviation of 5 sets of measurements where each measurement comprises 2-4 transects during three measurement days (12-Feb.-2018, 24-Apr.2018, and 07-Jan.-2019). Figure 7 shows an example of a fit of a Gaussian plume to the measurements from the Utrecht WWTP. The derived distance to the source was 215 ± 90 m, the hourly average wind speed was 3.5 ± 1.1 m s^{-1} and the wind direction was 178 ± 5 degrees (see SI, Sect. S.1.6, Table S5).

The total emission rate of the WWTP in Utrecht was estimated at 160 ± 90 t yr^{-1}. The reported errors include stability classes, wind speed and directions, and effective point source coordinates. Not all transects provided datasets that allowed an adequate Gaussian fit, these were not included in total estimates from the facilities, e.g. measurements during the visits of the harbor area in Hamburg were excluded. In Hamburg, plumes from several facilities were also intercepted several times (see SI, Sect. S.1.6, Table S6). For a Compost and Soil Company in Hamburg we estimate an emission rate of 70 ± 50 t yr^{-1}. The mobile quantifications at the upstream sites in Hamburg from a separator, a tank, and an oil well yield annual CH_4 emission of 4.5 ± 3.7 t yr^{-1}, 5.2 ± 3.0 t yr^{-1}, and 4.8 ± 4.0 t yr^{-1} respectively.

4 Discussion

4.1 Detection and quantification

As mentioned above (see Sect. 2.2.2), we used methods similar to the ones introduced by von Fischer et al. (2017) and updated in Weller et al. (2019) that were used to characterize CH_4 emission from local gas distribution systems in the US. An important difference is that we did not visit each street twice in the untargeted survey, and the revisits were specifically targeted at locations where we had found a LI during the first visit. A consequence of the different sampling strategy is that we do not base our city-level extrapolated emissions estimates on "confirmed" LIs, as done in Weller et al. (2019) but on all the LIs observed. In our study, 60 % of CH_4 LIs in Utrecht and 46 % of LIs in Hamburg were confirmed. This number may be biased high, since we preferentially revisited locations that had shown higher LIs, and the percentage of confirmed LIs may have been lower if we had visited locations with smaller LIs. Von Fischer et al. (2017) reported that LIs in the high emission rate category have a 74 % chance of detection, which decreased to 63 % for the middle category and 35 % frequency for the small category. In our study, all LIs within the high emission rate category (n = 1 and n = 2 LIs in Utrecht and Hamburg respectively) were confirmed in both cities. Overall, the confirmation rates found in Hamburg and Utrecht were similar to the ones reported in the US cities by von Fischer et al. (2017), suggesting that the results from both driving strategies can be compared when we take into account an overall confirmation percentage of roughly 50 %.

In 13 US cities the "LI density" ranged from 1 LI per 1.6 km driven to 1 LI per ≈ 320 km driven (EDF, 2019). This illustrates that cities within one country can be very different in their NGDN infrastructure. In Utrecht, one LI was observed every 5.6 km of street covered and in Hamburg every 8.4 km covered. Note that we normalize the number of LIs per km of road covered, not km of road driven, since the revisits were targeted to confirm LIs, which would bias the statistics if we normalize by km of road driven. After accounting for the confirmation percentage of 50 %, the LI densities in Utrecht and Hamburg become 1 LI per 11.2 km covered in Utrecht, and 1 LI per 16.8 km covered in Hamburg. When we take into account the attributions (fraction fossil/total LIs is 43 % in Utrecht and 31 % in Hamburg), confirmed LIs from the NGDN are found

every 26 km in Utrecht and every 54 km in Hamburg. The highest 1 % of the LIs in Utrecht and Hamburg account for approximately 30 % of emissions, emphasizing the presence of a skewed distribution of emissions. The emissions distribution is even more skewed for these two European cities than for countrywide US cities, where approximately 25 % of emissions comes from the highest 5 % of the LIs. Skewed emission distributions appear to be typical for emissions from the oil and gas supply chain across different scales. For example, a synthesis study reviewing the distribution of upstream emissions from the US natural gas system shows that in the US 5 % of the leaks are responsible for 50 % of the emissions (Brandt et al., 2016).

4.2 Attribution

Four different approaches were combined in Hamburg for emission source attribution, which allows an evaluation of their molecular consistency. Figure 5 shows that measurements of the C_2:C_1, δD, and $\delta^{13}C$ provide a very consistent distinction between fossil and microbial sources of CH_4. Except for one outlier with a very enriched $\delta^{13}C$ and δD contents and no C_2H_6 signal, all samples that are classified as "microbial" and depleted in $\delta^{13}C$ and δD signatures contain no measurable C_2H_6. Samples that are characterized as "fossil", based on $\delta^{13}C$ and δD signatures, bear a C_2H_6 concomitant signal. This strengthens the confidence in source attribution using these tracers. The fossil $\delta^{13}C$ signature of bag samples from natural gas leaks in Hamburg ($\delta^{13}C$ = -41.9 ± 1.0 ‰) is higher than recent reports from the city of Heidelberg, Germany ($\delta^{13}C$ = −43.3 ± 0.8 ‰ (Hoheisel et al., 2019)). This shows that within one country, $\delta^{13}C$ from NGDNs can vary from one region to another. These numbers do not agree within combined errors, but are also not very different. $\delta^{13}C$ values of CH_4 from the NGDN can vary regionally and temporally, e.g. due to differences in the mixture of natural gas from various suppliers for different regions in Germany (DVGW, 2013). In a comprehensive study at global scale, it is also shown that how $\delta^{13}C$ values of fossil fuel CH_4 have significant variabilities in different regions within an individual basin (Figure 4 in Sherwood et al. (2017)).

In Hamburg both C_2:C_1 and CH_4:CO_2 analysis along with $\delta^{13}C$ and δD signatures suggest that ≈ 50 % to ≈ 80 % of estimated emissions (≈ 30 % and ≈ 40 % of LIs respectively) originate from NGDNs, whereas CH_4:CO_2 analysis and the smaller sample of C_2:C_1 measurements in Utrecht suggests that the overwhelming fraction (70 - 90 % of emissions; 40 – 70 % of LIs) originated from NGDNs. We note that although it is widely assumed that microbial CH_4 is not associated with ethane, some studies have reported microbial production of ethane, so it may not be a unique identifier (Davis and Squires, 1954; Fukuda et al., 1984; Gollakota and Jayalakshmi, 1983; Formolo, 2010). The online C_2:C_1 analysis to attribute LIs is fast and can be used at larger scale, but with the instrument we used we were not able to clearly attribute sources with CH_4 enhancements of less than 500 ppb. Isotopic analysis by IRMS can attribute sources for smaller LIs (down to 100-200 ppb) but is clearly more labor intensive, and it would be a considerable effort to take samples from all LIs observed across an urban area. Overall, C_2H_6 and CO_2 signals are very useful in eliminating non-fossil LIs in mobile urban measurements and with improvements in instrumentations, analyzing signals of these two species along with evaluation of CH_4 signals can make process of detecting pipeline leaks from NGDN more efficient.

In Hamburg, most of the LIs were detected in the city center (Figure 1). This means that the LI density is higher than the average value in the center, but much lower than the average value in the surrounding districts and residential areas. Many of the LIs in the city center were attributed to combustion and microbial sources, thus they do not originate from leaks in the NGDN. Many of the microbial LIs encountered in Hamburg are around the Binnenalster lake (see SI, Sect. S.3.3, Figure S15), which suggests that anaerobic methanogenesis (Stephenson and Stickland, 1933; Thauer, 1998) can cause these microbial emission in this lake, as seen in other studies focused on emissions from other lakes (e.g., DelSontro et al., 2018; Townsend-Small et al., 2016). Microbial CH_4 emissions from sewage system (Guisasola et al., 2008) can also be an important source of in this area, as seen in US urban cities (Fries et al., 2018). Fries et al. (2018) performed direct measurement of CH_4 and nitrous oxide (N_2O) from a total of 104 sites, and analyzed $\delta^{13}C$ and δD signatures of samples from 27 of these locations, and attributed 47 % of these locations to microbial emissions in Cincinnati, Ohio, USA.

4.3 Comparison to national inventory reports

In the national inventory reports, total upscaled emissions from NGDNs are based on sets of emission factors for different pipeline materials (e.g., grey cast iron, steel, or plastic) at different pressures (e.g., <= 200 mbar or >200 mbar). The reported emission factors are based on IPCC tier 3 approach (Buendia et al., 2019). However, emission estimates do not exist for individual cities including Utrecht and Hamburg. Also, it is not possible to calculate a robust city-level estimate using the nationally reported emission factors because there is no publicly available associated activity data, i.e., pipeline materials and lengths for each material, at the level of individual cities. As a result, a robust direct comparison between nationally reported emissions and our measurements, akin to a recent study in the United States (Weller et al., 2020), is currently not possible. The following juxtaposition of our estimates and national inventory downscaling to city-level is therefore provided primarily as illustration of the data gaps rather than a scientific comparison. In Utrecht, we attributed 70 – 90 % of the mobile measurement inferred emissions of ≈ 150 t yr^{-1} to the NGDN, thus 105 – 135 t yr^{-1}.

The Netherlands National Institute for Public Health and the Environment (RIVM) inventory report derived an average NGDN emission factor of ≈ 110 kg km^{-1} yr^{-1} using 65 leak measurements from different pipeline materials and pressures in 2013. This weighted average ranged from a maximum of 230 kg km^{-1} yr^{-1} for grey cast iron pipelines to a minimum of 40 kg km^{-1} yr^{-1} for pipelines of other materials with overpressures <= 200 mbar (for details, see P. 130 in Peek et al. (2019)). This results in an average CH_4 emissions of ≈ 70 t yr^{-1} (min = 30 t yr^{-1} and max = 150 t yr^{-1}) for the study area of Utrecht, assuming ≈ 650 km of pipelines inside the ring, and further assuming that Utrecht's NGDN is representative of the national reported average (see qualifiers above). The average emissions for the Utrecht study, based on emissions factors reported for the Netherlands, is smaller by a factor of 1.5 - 2 compared to the emissions derived here. The variability factor of 5, from the reported emission (resulting from the variability in pipeline materials) highlights the need for city-level specific activity data for a robust comparison. In Hamburg, 50 – 80 % of the upscaled emissions of 440 t yr^{-1} (220 – 350 t yr^{-1}), can be attributed to the emission from NGDN. The national inventory from the Federal Environment Agency (UBA) in Germany, reports an average CH_4 emission factor for NGDN from low pressure pipelines as ≈ 290 kg km^{-1} yr^{-1} (max = 445 kg km^{-1} yr^{-1} (grey cast iron) and min = 51 kg km^{-1} yr^{-1} (plastic)) based on measurements from the 1990s (Table 169 in Federal Environment Agency (2019)). Assuming ≈ 3000 km of pipelines in the targeted region, and further assuming that Hamburg's NGDN is representative of the national reported average (see qualifiers above), results in an estimated NGDN CH_4 emissions average of ≈ 870 t yr^{-1} (min = 155 t yr^{-1} and max = 1350 t yr^{-1}). While this study's estimate (220 – 350 t yr^{-1}) falls in the lower end of this range, the reported emissions variability factor of 9 (resulting from the variability in pipeline materials) highlights again the need for city-level specific activity data for a robust comparison. To put the national inventory comparison into perspective, it should be noted that GasNetz Hamburg detected and fixed leaks at 20 % of the fossil LIs in this study, which accounted for 50 % of emissions. In Utrecht and Hamburg, the natural gas consumption in our target area were retrieved through communications with LDCs. In the Utrecht and Hamburg study areas, natural gas consumption is 0.16 bcm yr^{-1} (STEDIN, personal communication) and 0.75 bcm yr^{-1} (GasNetz Hamburg, personal communication) respectively. The estimated emissions from NGDNs in our study is between 0.10 – 0.12 % in Utrecht and between 0.04 – 0.07 % in Hamburg of total the annual natural gas consumptions in the same area. In the US, where the majority of natural gas consumption is from residential and commercial sectors, Weller et al. (2020) reported emissions of 0.69 Tg $year^{-1}$ (0.25 - 1.23 with 95 % confidence interval), with a sum of ≈ 170 Tg $year^{-1}$ (U.S. EIA, 2019), showing 0.4 % (0.15 % - 0.7 %) loss from NGDNs. The US NGDNs loss is about four times larger than our reported loss in Utrecht, and is about ten times larger than the loss for Hamburg. Considering the population of Utrecht (≈ 0.28 million) and Hamburg (≈ 1.45 million), the natural gas consumption densities in these study areas are ≈ 570 m^3 $capita^{-1}$ yr^{-1} and ≈ 520 m^3 $capita^{-1}$ yr^{-1}, where in the US (population ≈ 330 million (US Census Bureau, 2020)) the density is about ≈ 730 m^3 $capita^{-1}$ yr^{-1} (see SI, Sect. S.3.2, Figure S14). This shows that annual natural gas consumption per capita in the US is about 30 % and 40 % higher than in Utrecht and Hamburg respectively. The emission per

602 km of pipeline in Utrecht is between 0.45 – 0.5 L min^{-1} km^{-1} and in Hamburg is between 0.2 – 0.32 L min^{-1} km^{-1}. In the US,
603 based on 2,086,000 km km of local NGDN pipeline (Weller et al., 2020), this emission factor will be between 0.32 – 1.57 L
604 min^{-1} km^{-1}. This shows higher emissions per km pipeline in the countrywide studies of US compared to just two European
605 cities of Utrecht and Hamburg (see qualifiers above). This can be partly explained by pipeline material, maintenance protocols,
606 and higher use of natural gas consumption in the US. However, the substantial variability in emission rates across US cities,
607 as wells as the annual variability of gas consumption over the year, again restricts a direct comparison of two cities with a
608 national average measured over multiple years.
609 Normalized LIs emissions per capita in Utrecht (0.54 ± 0.15 kg yr^{-1} $capita^{-1}$) are almost double the emission factor in
610 Hamburg (0.31 ± 0.04 kg yr^{-1} $capita^{-1}$). This metric may be useful to compare cities, assuming that the emission quantification
611 method is equally effective for different cities. CH_4 emissions can vary among different cities, depending on the age,
612 management and material of NGDNs, and/or the management of local sewer systems. In our study, we only surveyed two
613 cities, and the above number may not be adequate for extrapolation to the country scale (McKain et al., 2015).

614 **4.4 Interaction with utilities**

615 After the city surveys, locations with the highest emissions (high and medium categories) were shared with STEDIN
616 Utrecht and all LI locations were reported to GasNetz Hamburg. The utilities repair teams were sent to check whether LIs
617 could be detected as leaks from NGDN and fixed. The LDCs follow leak detection procedures based on country regulations
618 (e.g., for GasNetz Hamburg in SI, Sect. S.4.1, Table S11). GasNetz Hamburg also co-located the coordinates of the detected
619 reported LIs with the NGDN and prioritized repairs based on safety regulations mentioned in Table S12 (see SI, Sect. S.4.1).
620 This interaction with the LDCs resulted in fixing major NGDN leaks in both cities. In Utrecht the only spot in the high emission
621 category was reported to STEDIN, but the pipelines on this street had been replaced, which most likely fixed the leak, as it
622 was not found later by the gas company nor in our later survey with the CH_4 - C_2H_6 analyzer. In Utrecht, half of the LIs in the
623 medium category were found and repaired.
624 A routine leak survey (detection and repair) had been performed by GasNetz Hamburg between 1-5 months before
625 the campaign, for the different regions (see SI, Sect. S.4.1., Table S11). The timing of any routine detection and repair likely
626 influences the absolute number of LIs measured during independent mobile measurements, and the survey by GasNetz
627 Hamburg thus likely has influenced the absolute number of LIs measured in our campaign. We then reported the LI
628 latitude/longitude coordinates to GasNetz Hamburg about 4 months after our campaign. Additionally, we provided map images
629 of the LIs immediately after the campaign. The comparison of the number of reported LIs (and emission rates) during our
630 campaign with those identified by GasNetz Hamburg post-campaign assumes that the leaks continued to emit gas until they
631 were detected and fixed by GasNetz Hamburg (if they were detected).
632 Depending on how close the gas leaks are located to a building, the LDCs prioritize the leaks into four classes from
633 the highest to lowest priority: A1, A2, B, and C (see SI, Sect. S.4.1, Table S12). In Hamburg, both LIs in the high category
634 were identified as A1 gas leaks and fixed by GasNetz Hamburg immediately. Most of the Hamburg LIs that were detected and
635 identified as fossil are in close proximity to the natural gas distribution pipelines (see SI, Sect. S.4.2, Table S13). Investigation
636 of the pipeline material shows that most of NGDN emissions are due to leaks from steel pipelines (see SI, Sect. S.4.2, Table
637 S14), which are more prone to leakage because of pipeline corrosion (Zhao et al., 2018). Nevertheless, only 7 of the 30 LIs
638 (23 %) that were positively attributed to fossil CH_4 were detected and fixed by the LDC. If we assume that the fraction fossil
639 / total LIs determined in Hamburg (≈ 35 %) is representative for the entire population of LIs encountered (thus also for the
640 ones that were not attributable), about 50 of the 145 LIs are likely due to fossil CH_4. The LDC found and fixed leaks at 10 of
641 these locations (≈ 20 %). A recent revisit (January 2020) to these locations confirmed that no LIs were detected at 9 out of
642 these 10 locations. For the 10^{th} location a smaller LI was detected in close proximity, and GasNetz Hamburg confirmed that

this was a leak from a steel pipeline. The whole pipeline system on this street dates back to the 1930s and is targeted for replacement in the near future.

In summary, about 20 % of the LIs including the two largest LIs that were attributed to a fossil source were identified as NGDN gas leaks (see SI, Sect. S.4.2, Figure S18), and were repaired by GasNetz Hamburg, but these accounted for about 50 % of fossil CH_4 emissions of Hamburg, similar to what was observed in the US studies (Weller et al., 2018). Possibly, smaller leakages that can be detected with the high sensitivity instruments used in the mobile surveys cannot be detected with the less sensitive equipment of LDCs. Another possible explanation for the fact that the LDC did not detect more leaks may be that reported LI locations do not always coincide with the actual leak locations, although Weller et al. (2018) reported that the median distance of actual leak locations to the reported ones was 19 m. Combined measurements with GasNetz Hamburg are planned to investigate why the majority of the smaller LIs reported in mobile surveys is not detected in the regular surveys of the LDC.

The average C_2:C_1 ratio for LIs with a significant C_2H_6 signals across Hamburg was 5.6 ± 3.9 %. For the spots where the LDC found and fixed leaks this ratio was 3.9 ± 2.6 %. Thus, some of the locations where CH_4 enhancements were found were influenced by sources with an even higher C_2:C_1 ratio than the gas in the NGDN. One confirmed example is the very high ratio found in exhaust from a vehicle as shown in Figure S12 (see SI, Sect. S.2.6). The abnormal operation of this vehicle is confirmed by the very high CH_4:CO_2 ratio of 5.5 ppb:ppm (SI, section S2). This is more than 20 times higher than CH_4:CO_2 ratios of 0.2 ± 0.1 ppb:ppm observed during passages through the Elbe tunnel, a ratio that agrees with previous studies (SI, section S2).

Repairing gas leaks in a city has several benefits for safety (preventing explosions), sustainability (minimizing GHG emissions) and economics. Gas that is not lost via leaks can be sold for profit, but gas leak detection and repair is expensive and is usually associated with interruptions of the infrastructure (breaking up pavements and roads). Also, as reported above, and in agreement with the studies in US cities, for small LIs the underlying leaks are often not found by the LDCs, possibly because their equipment is less sensitive and aimed for finding leak rates that are potentially dangerous.

Our measurements in Hamburg demonstrate that in particular smaller LIs may originate from biogenic sources, e.g. the sewage system, and not necessarily from leaks in the NGDN. In this respect, attribution of LIs prior to reporting to the LDCs may be beneficial to facilitate effective repair. Figure S19 (see SI, Sect. S.5) illustrates how the individual measurement components can be efficiently combined in a city leak survey program.

4.5 Large facilities

The WWTP in Utrecht emits 160 ± 90 t yr^{-1}, which is similar to the total detected emissions (150 t yr^{-1}) inside the study area of Utrecht. The emissions reported for this facility from 2010 until 2017 are 130 ± 50 t yr^{-1} (Rijksoverheid, 2019), in good agreement with our measurements. CH_4 emission from a single well in Hamburg was estimated at 4.4 ± 3.5 t yr^{-1}, which is in the range of median emissions of 2.3 t yr^{-1} reported for gas production wells in Groningen, NL (Yacovitch et al., 2018), and average emissions of all US oil and gas production wells 7.9 ± 1.8 t yr^{-1} (Alvarez et al., 2018). In Hamburg, the emissions from a Compost and Soil Company amount to about 10 % of the total emissions in the city target region, whereas a wellhead, a storage tank and a waste-oil separator contribute only about 1 % each. This shows that individual facilities can contribute significantly to the total emissions of a city. The contribution of each source is dependent on infrastructure, urban planning and other conditions in the city (e.g. age and material of pipeline, maintenance programs, waste management, sewer system conditions, etc.), which may change the source mix from one city to another. For example, in Utrecht the WWTP is located within our domain of study. The wastewater treatment in Hamburg most likely causes CH_4 emissions elsewhere. Therefore, facility-scale CH_4 emissions should be reported on a more aggregated provincial or national level. For emissions from the NGDN, the urban scale is highly relevant, as the emission can only be mitigated at this scale.

5 Conclusions

Mobile measurements provide a fast and accurate technique for observing and identifying even relatively small CH_4 enhancements (i.e., tens of ppb) across cities and are useful for detecting potential gas leaks. During our intensive measurement campaigns, 81 LIs were observed in Utrecht (corresponding to emissions of ≈110 t CH_4 yr^{-1}) and 145 LIs (≈180 t CH_4 yr^{-1}) in Hamburg. These estimates, based on the streets covered, were then up-scaled to the total study area, using the road network map as a proxy for the length of the pipeline network which then yielded total emissions of 150 t yr^{-1} and 440 t yr^{-1} across the study area of Utrecht and Hamburg respectively. The isotopic signature of CH_4 in air samples and continuous mobile measurement of CO_2 and C_2H_6 mole fraction show that not all the LIs observed across the two cities have fossil origin. In Utrecht, C_2:C_1 and CH_4:CO_2 analyses show that 70 -90 % of emissions were fossil. In Hamburg, C_2:C_1, CH_4:CO_2, and $\delta^{13}C$-δD analyses suggests that 50 - 80 % of emissions originate from natural gas pipelines. For the locations where samples for isotope analysis were collected, 80 % of emissions were identified as fossil. A large fraction of emissions in both cities originated from few high emitting locations. The LDC in Hamburg (GasNetz Hamburg) detected and fixed leaks at 20 % of the locations that likely due to fossil sources, but these accounted for 50 % of emissions. Large LIs were generally confirmed as gas leaks from steel pipelines. The C2:C1 ratio at the locations where gas leaks were fixed by GasNetz Hamburg was 3.9 ± 2.6 %. The mobile measurement technique is less labor and time intensive than conventional methods and can provide extensive coverage across a city in a short period. Based on our experience for the Netherlands and Germany a protocol could be developed that aids LDCs in guiding their leak detection and repair teams. The use of emission categories and source attribution can help target repair activities to the locations of large fossil emissions. Emission quantification from large facilities shows that these emissions may be equivalent to total CH_4 emissions from NGDN leaks in urban environments. In order to analyze discrepancies between spatial explicit measurement-based estimates as presented here with reported annual average national emissions by sectors a coordinated effort with national agencies is necessary to address the lack of publicly available activity data (e.g., pipe material) disaggregated from the national-level (e.g., at the city-level).

Author contributions

H. M. performed the mobile measurements, wrote the MATLAB® code, analyzed the data, and together with T. R. drafted the manuscript. J. M. F. and M. M. contributed with air sampling and isotope analysis. D. Z. -A. and S. S. contributed to the scientific interpretation and comparison between European and US cities. Z. D. W. and J. C. v. F. facilitated comparison to US cities and contributed to the statistical analysis. H. D. v. d. G. and T. R. provided instruments, equipment, and supervised the measurements and data analysis. T. R. developed the research idea and coordinated the city campaigns. All authors contributed to the interpretation of the results and the improvement of the manuscript.

Competing interests: The authors declare that they have no conflict of interest.

Acknowledgements

This work was supported by the Climate and Clean Air Coalition (CCAC) Oil and Gas Methane Science Studies (MMS) hosted by the United Nations Environment Programme. Funding was provided by the Environmental Defense Fund, Oil and Gas Climate Initiative, European Commission, and CCAC. This project received further support from the H2020 Marie Skłodowska-Curie project Methane goes Mobile – Measurements and Modelling ($MEMO^2$; https://h2020-memo2.eu/), grant number 722479. Dr. Daniel Zavala-Araiza and Dr. Stefan Schwietzke were funded by the Robertson Foundation. We thank Dr. Rebecca Fisher who supervised RHUL contribution to the isotopic analysis of Hamburg campaign. Special thanks to Prof. Stefan Bühler from the Meteorological Institute of Hamburg University and Dr. Stefan Kinne from the Max Planck Institute for Meteorology for hosting our team during the Hamburg city measurement surveys. We would like to extend our appreciation

to the anonymous referees for the insightful comments which led to improvements of the manuscript. We appreciate continuous efforts from executive and management boards of GasNetz Hamburg, Dr. Luise Westphal, Michael Dammann, Dr. Ralf Luy, and Christian Feickert who facilitated productive communications, provided information on the gas infrastructure in Hamburg and organized leaks repairs with their teams in study area of Hamburg. We also thank asset manager of STEDIN Utrecht, Ricardo Verhoeve who provided information and planned leaks repairs by STEDIN in Utrecht. We thank Charlotte Große from DBI Gas and Environmental Technologies GmbH Leipzig (DBI GUT Leipzig) who helped with clarifying information on reported emission factors provided in national inventory reports. We thank the former MSc students of Utrecht University, Laurens Stoop and Tim van den Akker who helped with the measurements in Utrecht study area.

References

ACM: Authority for Consumers and Markets in the Netherlands, Low NOx Burgners (LNBs) gas code, [online] Available from: https://wetten.overheid.nl/BWBR0037935/2018-05-26, 2018.

Allen, D. T., Torres, V. M., Thomas, J., Sullivan, D. W., Harrison, M., Hendler, A., Herndon, S. C., Kolb, C. E., Fraser, M. P., Hill, A. D., Lamb, B. K., Miskimins, J., Sawyer, R. F. and Seinfeld, J. H.: Measurements of methane emissions at natural gas production sites in the United States, Proc. Natl. Acad. Sci., 110(44), 17768–17773, doi:10.1073/pnas.1304880110, 2013.

Alvarez, R. A., Zavala-Araiza, D., Lyon, D. R., Allen, D. T., Barkley, Z. R., Brandt, A. R., Davis, K. J., Herndon, S. C., Jacob, D. J., Karion, A., Kort, E. A., Lamb, B. K., Lauvaux, T., Maasakkers, J. D., Marchese, A. J., Omara, M., Pacala, S. W., Peischl, J., Robinson, A. L., Shepson, P. B., Sweeney, C., Townsend-Small, A., Wofsy, S. C. and Hamburg, S. P.: Assessment of methane emissions from the U.S. oil and gas supply chain., Science, 361(6398), 186–188, doi:10.1126/science.aar7204, 2018.

Brandt, A. R., Heath, G. A. and Cooley, D.: Methane Leaks from Natural Gas Systems Follow Extreme Distributions, Environ. Sci. Technol., 50(22), 12512–12520, doi:10.1021/acs.est.6b04303, 2016.

Brantley, H. L., Hagler, G. S. W., Kimbrough, E. S., Williams, R. W., Mukerjee, S. and Neas, L. M.: Mobile air monitoring data-processing strategies and effects on spatial air pollution trends, Atmos. Meas. Tech., 7(7), 2169–2183, doi:10.5194/amt-7-2169-2014, 2014.

Brass, M. and Röckmann, T.: Continuous-flow isotope ratio mass spectrometry method for carbon and hydrogen isotope measurements on atmospheric methane, Atmos. Meas. Tech., 3(6), 1707–1721, doi:10.5194/amt-3-1707-2010, 2010.

Bright, E. A., Coleman, P. R. and Dobson, J. E.: LandScan : A Global Population database for estimating populations at risk, [online] Available from: https://www.semanticscholar.org/paper/LandScan-%3A-A-Global-Population-database-for-at-risk-Bright-Coleman/17e6076b6761788684434d1e14e85e8877fc0146 (Accessed 23 September 2019), 2000.

Brümmer, B., Lange, I. and Konow, H.: Atmospheric boundary layer measurements at the 280 m high Hamburg weather mast 1995-2011: mean annual and diurnal cycles, Meteorol. Zeitschrift, 21(4), 319–335, doi:10.1127/0941-2948/2012/0338, 2012.

Buendia, E. C., Guendehou, S., Limmeechokchai, B., Pipatti, R., Rojas, Y., Sturgiss, R., Tanabe, K., Wirth, T., Romano, D., Witi, J., Garg, A., Weitz, M. M., Cai, B., Ottinger, D. A., Dong, H., MacDonald, J. D., Ogle, S. M., Rocha, M. T., Sanchez, M. J. S., Bartram, D. M. and Towprayoon, S.: 2019 refinement to the 2006 IPCC guidelines for national greenhouse gas inventories. [online] Available from: https://www.ipcc.ch/report/2019-refinement-to-the-2006-ipcc-guidelines-for-national-greenhouse-gas-inventories/, 2019.

Bukowiecki, N., Dommen, J., Prévôt, A. S. H., Richter, R., Weingartner, E. and Baltensperger, U.: A mobile pollutant measurement laboratory - Measuring gas phase and aerosol ambient concentrations with high spatial and temporal resolution, Atmos. Environ., 36(36–37), 5569–5579, doi:10.1016/S1352-2310(02)00694-5, 2002.

Caulton, D. R., Li, Q., Bou-Zeid, E., Fitts, J. P., Golston, L. M., Pan, D., Lu, J., Lane, H. M., Buchholz, B., Guo, X., McSpiritt, J., Wendt, L. and Zondlo, M. A.: Quantifying uncertainties from mobile-laboratory-derived emissions of well pads using inverse Gaussian methods, Atmos. Chem. Phys., 18(20), 15145–15168, doi:10.5194/acp-18-15145-2018, 2018.

Chamberlain, S. D., Ingraffea, A. R. and Sparks, J. P.: Sourcing methane and carbon dioxide emissions from a small city: Influence of natural gas leakage and combustion, Environ. Pollut., 218, 102–110, doi:10.1016/J.ENVPOL.2016.08.036, 2016.

Chen, J., Dietrich, F., Maazallahi, H., Forstmaier, A., Winkler, D., Hofmann, M. E. G., Denier van der Gon, H. and Röckmann, T.: Methane emissions from the Munich Oktoberfest, Atmos. Chem. Phys., 20(6), 3683–3696, doi:10.5194/acp-20-3683-2020, 2020.

Curran, S. J., Wagner, R. M., Graves, R. L., Keller, M. and Green, J. B.: Well-to-wheel analysis of direct and indirect use of natural gas in passenger vehicles, Energy, 75, 194–203, doi:10.1016/j.energy.2014.07.035, 2014.

Davis, J. B. and Squires, R. M.: Detection of Microbially Produced Gaseous Hydrocarbons Other than Methane., Science, 119(3090), 381–2, doi:10.1126/science.119.3090.381, 1954.

DelSontro, T., Beaulieu, J. J. and Downing, J. A.: Greenhouse gas emissions from lakes and impoundments: Upscaling in the face of global change, Limnol. Oceanogr. Lett., 3(3), 64–75, doi:10.1002/lol2.10073, 2018.

DVGW: Technische Regel – ArbeitsblattDVGW G 260 (A), Bonn. [online] Available from: https://shop.wvgw.de/var/assets/leseprobe/508866_lp G 260.pdf, 2013.

E. K. Nam, T. E. Jensen, A. and Wallington, T. J.: Methane Emissions from Vehicles, Environ. Sci. Technol., doi:10.1021/ES034837G, 2004.

EDF: Local leaks impact global climate, [online] Available from: https://www.edf.org/climate/methanemaps (Accessed 5 November 2019), 2019.

Efron, B.: Bootstrap Methods: Another Look at the Jackknife, Ann. Stat., 7(1), 1–26, doi:10.1214/aos/1176344552, 1979.

Efron, B.: The Jackknife, the Bootstrap and Other Resampling Plans, Society for Industrial and Applied Mathematics., 1982.

Efron, B. and Tibshirani, R. J.: An Introduction to the Bootstrap, Champman & Hall, London., 1993.

EPA: User's guide for the industrial source guide complex (ISC3) dispersion models, volume II - Description of model algorithms., 1995.

Etheridge, D. M., Steele, L. P., Francey, R. J. and Langenfeld, R. L.: Atmospheric methane between 1000 A.D. and present: Evidence of anthropogenic emissions and climatic variability, J. Geophys. Res., 103, 979–993, doi:0148-0227/98/98JD-00923, 1998.

Etminan, M., Myhre, G., Highwood, E. J. and Shine, K. P.: Radiative forcing of carbon dioxide, methane, and nitrous oxide: A significant revision of the methane radiative forcing, Geophys. Res. Lett., 43(24), 12,614-12,623, doi:10.1002/2016GL071930@10.1002/(ISSN)1944-8007.2016GRLEDHIGH, 2016.

Federal Environment Agency: National Inventory Report for the German Greenhouse Gas Inventory 1990 – 2017. [online] Available from: https://unfccc.int/documents/194930, 2019.

von Fischer, J. C., Cooley, D., Chamberlain, S., Gaylord, A., Griebenow, C. J., Hamburg, S. P., Salo, J., Schumacher, R., Theobald, D. and Ham, J.: Rapid, Vehicle-Based Identification of Location and Magnitude of Urban Natural Gas Pipeline Leaks, Environ. Sci. Technol., 51(7), 4091–4099, doi:10.1021/acs.est.6b06095, 2017.

Fisher, R., Lowry, D., Wilkin, O., Sriskantharajah, S. and Nisbet, E. G.: High-precision, automated stable isotope analysis of atmospheric methane and carbon dioxide using continuous-flow isotope-ratio mass spectrometry, Rapid Commun. Mass Spectrom., 20(2), 200–208, 2006.

Fisher, R. E., Sriskantharajah, S., Lowry, D., Lanoisellé, M., Fowler, C. M. R., James, R. H., Hermansen, O., Lund Myhre, C., Stohl, A., Greinert, J., Nisbet-Jones, P. B. R., Mienert, J. and Nisbet, E. G.: Arctic methane sources: Isotopic evidence for atmospheric inputs, Geophys. Res. Lett., 38(21), n/a-n/a, doi:10.1029/2011GL049319, 2011.

Formolo, M.: The Microbial Production of Methane and Other Volatile Hydrocarbons, in Handbook of Hydrocarbon and Lipid Microbiology, pp. 113–126, Springer Berlin Heidelberg., 2010.

France, J. L., Cain, M., Fisher, R. E., Lowry, D., Allen, G., O'Shea, S. J., Illingworth, S., Pyle, J., Warwick, N., Jones, B. T., Gallagher, M. W., Bower, K., Le Breton, M., Percival, C., Muller, J., Welpott, A., Bauguitte, S., George, C., Hayman, G. D., Manning, A. J., Myhre, C. L., Lanoisellé, M. and Nisbet, E. G.: Measurements of $\delta^{13}C$ in CH_4 and using particle dispersion modeling to characterize sources of Arctic methane within an air mass, J. Geophys. Res. Atmos., 121(23), 14,257-14,270, doi:10.1002/2016JD026006, 2016.

Fries, A. E., Schifman, L. A., Shuster, W. D. and Townsend-Small, A.: Street-level emissions of methane and nitrous oxide from the wastewater collection system in Cincinnati, Ohio, Environ. Pollut., 236, 247–256, doi:10.1016/j.envpol.2018.01.076, 2018.

Fukuda, H., Fujii, T. and Ogawa, T.: Microbial Production of C_2 -Hydrocarbons, Ethane, Ethylene and Acetylene, Agric. Biol. Chem., 48(5), 1363–1365, doi:10.1080/00021369.1984.10866323, 1984.

Gallagher, M. E., Down, A., Ackley, R. C., Zhao, K., Phillips, N. and Jackson, R. B.: Natural Gas Pipeline Replacement Programs Reduce Methane Leaks and Improve Consumer Safety, Environ. Sci. Technol. Lett., 2(10), 286–291, doi:10.1021/acs.estlett.5b00213, 2015.

Gioli, B., Toscano, P., Lugato, E., Matese, A., Miglietta, F., Zaldei, A. and Vaccari, F. P.: Methane and carbon dioxide fluxes and source partitioning in urban areas: The case study of Florence, Italy, Environ. Pollut., 164, 125–131, doi:10.1016/j.envpol.2012.01.019, 2012.

Gollakota, K. G. and Jayalakshmi, B.: Biogas (natural gas?) production by anaerobic digestion of oil cake by a mixed culture isolated from cow dung, Biochem. Biophys. Res. Commun., 110(1), 32–35, doi:10.1016/0006-291X(83)91255-X, 1983.

Guisasola, A., de Haas, D., Keller, J. and Yuan, Z.: Methane formation in sewer systems, Water Res., 42(6–7), 1421–1430, doi:10.1016/j.watres.2007.10.014, 2008.

Heilig, G. K.: The greenhouse gas methane (CH4): Sources and sinks, the impact of population growth, possible interventions, Popul. Environ., 16(2), 109–137, doi:10.1007/BF02208779, 1994.

Helfter, C., Tremper, A. H., Halios, C. H., Kotthaus, S., Bjorkegren, A., Sue, C., Grimmond, B., Barlow, J. F. and Nemitz, E.: Spatial and temporal variability of urban fluxes of methane, carbon monoxide and carbon dioxide above London, UK, Atmos. Chem. Phys, 16, 10543–10557, doi:10.5194/acp-16-10543-2016, 2016.

Helmig, D., Rossabi, S., Hueber, J., Tans, P., Montzka, S. A., Masarie, K., Thoning, K., Plass-Duelmer, C., Claude, A., Carpenter, L. J., Lewis, A. C., Punjabi, S., Reimann, S., Vollmer, M. K., Steinbrecher, R., Hannigan, J. W., Emmons, L. K., Mahieu, E., Franco, B., Smale, D. and Pozzer, A.: Reversal of global atmospheric ethane and propane trends largely due to US oil and natural gas production, Nat. Geosci., 9(7), 490–495, doi:10.1038/ngeo2721, 2016.

Hendrick, M. F., Ackley, R., Sanaie-Movahed, B., Tang, X. and Phillips, N. G.: Fugitive methane emissions from leak-prone natural gas distribution infrastructure in urban environments, Environ. Pollut., 213, 710–716, doi:10.1016/j.envpol.2016.01.094, 2016.

Hmiel, B., Petrenko, V. V, Dyonisius, M. N., Buizert, C., Smith, A. M., Place, P. F., Harth, C., Beaudette, R., Hua, Q., Yang, B., Vimont, I., Michel, S. E., Severinghaus, J. P., Etheridge, D., Bromley, T., Schmitt, J., Faïn, X., Weiss, R. F. and Dlugokencky, E.: Preindustrial 14 CH 4 indicates greater anthropogenic fossil CH 4 emissions, Nature, 578, doi:10.1038/s41586-020-1991-8, 2020.

Hoheisel, A., Yeman, C., Dinger, F., Eckhardt, H. and Schmidt, M.: An improved method for mobile characterisation of δ^{13} CH_4 source signatures and its application in Germany, Atmos. Meas. Tech., 12(2), 1123–1139, doi:10.5194/amt-12-1123-2019, 2019.

Hopkins, F. M., Kort, E. A., Bush, S. E., Ehleringer, J. R., Lai, C.-T., Blake, D. R. and Randerson, J. T.: Spatial patterns and source attribution of urban methane in the Los Angeles Basin, J. Geophys. Res. Atmos., 121(5), 2490–2507, doi:10.1002/2015JD024429, 2016.

Hu, N., Liu, S., Gao, Y., Xu, J., Zhang, X., Zhang, Z. and Lee, X.: Large methane emissions from natural gas vehicles in Chinese cities, Atmos. Environ., 187, 374–380, doi:10.1016/j.atmosenv.2018.06.007, 2018.

IPCC: Guidelines for national greenhouse inventories. [online] Available from: https://www.ipcc-nggip.iges.or.jp/public/gl/guidelin/ch1ref8.pdf, 1996.

907 Jackson, R. B., Down, A., Phillips, N. G., Ackley, R. C., Cook, C. W., Plata, D. L. and Zhao, K.: Natural gas pipeline leaks
908 across Washington, DC, Environ. Sci. Technol., 48(3), 2051–2058, doi:10.1021/es404474x, 2014.
909 Karion, A., Sweeney, C., Pétron, G., Frost, G., Michael Hardesty, R., Kofler, J., Miller, B. R., Newberger, T., Wolter, S.,
910 Banta, R., Brewer, A., Dlugokencky, E., Lang, P., Montzka, S. A., Schnell, R., Tans, P., Trainer, M., Zamora, R. and
911 Conley, S.: Methane emissions estimate from airborne measurements over a western United States natural gas field,
912 Geophys. Res. Lett., 40(16), 4393–4397, doi:10.1002/grl.50811, 2013.
913 Keeling, C. D.: The concentration and isotopic abundances of atmospheric carbon dioxide in rural areas, Geochim.
914 Cosmochim. Acta, 13(4), 322–334, doi:10.1016/0016-7037(58)90033-4, 1958.
915 Keeling, C. D.: The concentration and isotopic abundances of carbon dioxide in rural and marine air, Geochim. Cosmochim.
916 Acta, 24(3–4), 277–298, doi:10.1016/0016-7037(61)90023-0, 1961.
917 Lamb, B. K., Cambaliza, M. O. L., Davis, K. J., Edburg, S. L., Ferrara, T. W., Floerchinger, C., Heimburger, A. M. F., Herndon,
918 S., Lauvaux, T., Lavoie, T., Lyon, D. R., Miles, N., Prasad, K. R., Richardson, S., Roscioli, J. R., Salmon, O. E.,
919 Shepson, P. B., Stirm, B. H. and Whetstone, J.: Direct and Indirect Measurements and Modeling of Methane
920 Emissions in Indianapolis, Indiana, Environ. Sci. Technol., 50(16), 8910–8917, doi:10.1021/acs.est.6b01198, 2016.
921 LBEG: Geoinformation of Lower Saxony and Schleswig-Holstein, [online] Available from: https://nibis.lbeg.de/cardomap3/,
922 2018.
923 Lebel, E. D., Lu, H. S., Speizer, S. A., Finnegan, C. J. and Jackson, R. B.: Quantifying Methane Emissions from Natural Gas
924 Water Heaters, Environ. Sci. Technol., 54(9), 5737–5745, doi:10.1021/acs.est.9b07189, 2020.
925 Lowry, D., Fisher, R. E., France, J. L., Coleman, M., Lanoisellé, M., Zazzeri, G., Nisbet, E. G., Shaw, J. T., Allen, G., Pitt, J.
926 and Ward, R. S.: Environmental baseline monitoring for shale gas development in the UK: Identification and
927 geochemical characterisation of local source emissions of methane to atmosphere, Sci. Total Environ., 708, 134600,
928 doi:10.1016/j.scitotenv.2019.134600, 2020.
929 Lyon, D. R., Zavala-Araiza, D., Alvarez, R. A., Harriss, R., Palacios, V., Lan, X., Talbot, R., Lavoie, T., Shepson, P.,
930 Yacovitch, T. I., Herndon, S. C., Marchese, A. J., Zimmerle, D., Robinson, A. L. and Hamburg, S. P.: Constructing
931 a Spatially Resolved Methane Emission Inventory for the Barnett Shale Region, Environ. Sci. Technol., 49(13), 8147–
932 8157, doi:10.1021/es506359c, 2015.
933 Lyon, D. R., Alvarez, R. A., Zavala-Araiza, D., Brandt, A. R., Jackson, R. B. and Hamburg, S. P.: Aerial Surveys of Elevated
934 Hydrocarbon Emissions from Oil and Gas Production Sites, Environ. Sci. Technol., 50(9), 4877–4886,
935 doi:10.1021/acs.est.6b00705, 2016.
936 Maazallahi, H., Fernandez, J. M., Menoud, M., Zavala-Araiza, D., Weller, Z. D., Schwietzke, S., von Fischer, J. C., Denier
937 van der Gon, H., and Röckmann, T.: MATLAB® code for evaluation of Urban Surveys, Zenodo, doi:
938 10.5281/zenodo.3928972, 2020a.
939 Maazallahi, H., Fernandez, J. M., Menoud, M., Zavala-Araiza, D., Weller, Z. D., Schwietzke, S., von Fischer, J. C., Denier
940 van der Gon, H., and Röckmann, T.: Utrecht and Hamburg city measurements data, ICOS,
941 https://doi.org/10.18160/RAJS-KZZQ, 2020b.
942 MacFarling Meure, C., Etheridge, D., Trudinger, C., Steele, P., Langenfelds, R., van Ommen, T., Smith, A. and Elkins, J.:
943 Law Dome CO2 , CH4 and N2O ice core records extended to 2000 years BP, Geophys. Res. Lett., 33(14), L14810,
944 doi:10.1029/2006GL026152, 2006.
945 McKain, K., Down, A., Raciti, S. M., Budney, J., Hutyra, L. R., Floerchinger, C., Herndon, S. C., Nehrkorn, T., Zahniser, M.
946 S., Jackson, R. B., Phillips, N. and Wofsy, S. C.: Methane emissions from natural gas infrastructure and use in the
947 urban region of Boston, Massachusetts, Proc. Natl. Acad. Sci., 112(7), 1941–1946, doi:10.1073/PNAS.1416261112,
948 2015.
949 Mitchell, A. L., Tkacik, D. S., Roscioli, J. R., Herndon, S. C., Yacovitch, T. I., Martinez, D. M., Vaughn, T. L., Williams, L.
950 L., Sullivan, M. R., Floerchinger, C., Omara, M., Subramanian, R., Zimmerle, D., Marchese, A. J. and Robinson, A.
951 L.: Measurements of Methane Emissions from Natural Gas Gathering Facilities and Processing Plants: Measurement
952 Results, Environ. Sci. Technol., 49(5), 3219–3227, doi:10.1021/es5052809, 2015.
953 Myhre, G., Shindell, D., Bréon, F. M., Collins, W., Fuglestvedt, J., Huang, J., Koch, D., Lamarque, J. F., Lee, D., Mendoza,
954 B., Nakajima, T., Robock, A., Stephens, G., Takemura, T. and Zhan, H.: Anthropogenic and Natural Radiative Forc-
955 ing. In: Climate Change 2013: The Physical Science Basis. Contribution of Working Group I to the Fifth Assessment
956 Report of the Intergovernmental Panel on Climate Change, Cambridge, United Kingdom and New York, NY, USA.
957 [online] Available from: https://www.ipcc.ch/site/assets/uploads/2018/02/WG1AR5_Chapter08_FINAL.pdf, 2013.
958 Naus, S., Röckmann, T. and Popa, M. E.: The isotopic composition of CO in vehicle exhaust, Atmos. Environ., 177, 132–142,
959 doi:10.1016/J.ATMOSENV.2018.01.015, 2018.
960 Neumann, G. and Halbritter, G.: Sensitivity analysis of the Gaussian plume model, in Studies in Environmental Science, vol.
961 8, pp. 57–62, Elsevier., 1980.
962 Noël, S., Weigel, K., Bramstedt, K., Rozanov, A., Weber, M., Bovensmann, H. and Burrows, J. P.: Water vapour and methane
963 coupling in the stratosphere observed using SCIAMACHY solar occultation measurements, Atmos. Chem. Phys.,
964 18(7), 4463–4476, doi:10.5194/acp-18-4463-2018, 2018.
965 O'Shea, S. J., Allen, G., Fleming, Z. L., Bauguitte, S. J.-B., Percival, C. J., Gallagher, M. W., Lee, J., Helfter, C. and Nemitz,
966 E.: Area fluxes of carbon dioxide, methane, and carbon monoxide derived from airborne measurements around
967 Greater London: A case study during summer 2012, J. Geophys. Res. Atmos., 119(8), 4940–4952,
968 doi:10.1002/2013JD021269, 2014.
969 Omara, M., Sullivan, M. R., Li, X., Subramanian, R., Robinson, A. L. and Presto, A. A.: Methane Emissions from

970 Conventional and Unconventional Natural Gas Production Sites in the Marcellus Shale Basin, Environ. Sci. Technol.,
971 50(4), 2099–2107, doi:10.1021/acs.est.5b05503, 2016.
972 Paredes, M. G., Güereca, L. P., Molina, L. T. and Noyola, A.: Methane emissions from anaerobic sludge digesters in Mexico:
973 On-site determination vs. IPCC Tier 1 method, Sci. Total Environ., 656, 468–474,
974 doi:10.1016/j.scitotenv.2018.11.373, 2019.
975 Peek, C. J., Montfoort, J. A., Dröge, R., Guis, B., Baas, K., Huet, B. van, Hunnik, O. R. van and Berghe, A. C. W. M. van den:
976 Methodology report on the calculation of emissions to air from the sectors Energy, Industry and Waste, as used by
977 the Dutch Pollutant Release and Transfer Register., 2019.
978 Phillips, N. G., Ackley, R., Crosson, E. R., Down, A., Hutyra, L. R., Brondfield, M., Karr, J. D., Zhao, K. and Jackson, R. B.:
979 Mapping urban pipeline leaks: Methane leaks across Boston, Environ. Pollut., 173, 1–4,
980 doi:10.1016/j.envpol.2012.11.003, 2013.
981 Popa, M. E., Vollmer, M. K., Jordan, A., Brand, W. A., Pathirana, S. L., Rothe, M. and Röckmann, T.: Vehicle emissions of
982 greenhouse gases and related tracers from a tunnel study: CO : CO2 , N2O : CO2 , CH4 : CO2 , O2 : CO2 ratios, and
983 the stable isotopes 13C and 18O in CO2 and CO, Atmos. Chem. Phys., 14(4), 2105–2123, doi:10.5194/acp-14-2105-
984 2014, 2014.
985 Prather, M. J., Holmes, C. D. and Hsu, J.: Reactive greenhouse gas scenarios: Systematic exploration of uncertainties and the
986 role of atmospheric chemistry, Geophys. Res. Lett., 39(9), n/a-n/a, doi:10.1029/2012GL051440, 2012.
987 Rijksoverheid: Emissieregstratie. [online] Available from: http://www.emissieregistratie.nl/erpubliek/erpub/facility.aspx
988 (Accessed 9 December 2019), 2019.
989 Röckmann, T., Eyer, S., van der Veen, C., Popa, M. E., Tuzson, B., Monteil, G., Houweling, S., Harris, E., Brunner, D.,
990 Fischer, H., Zazzeri, G., Lowry, D., Nisbet, E. G., Brand, W. A., Necki, J. M., Emmenegger, L. and Mohn, J.: In situ
991 observations of the isotopic composition of methane at the Cabauw tall tower site, Atmos. Chem. Phys., 16(16),
992 10469–10487, doi:10.5194/acp-16-10469-2016, 2016.
993 Schaum, C., Lensch, D., Bolle, P. Y. and Cornel, P.: Sewage sludge treatment: Evaluation of the energy potential and methane
994 emissions with cod balancing, J. Water Reuse Desalin., 5(4), 437–445, doi:10.2166/wrd.2015.129, 2015.
995 Schmidt, G. A. and Shindell, D. T.: Atmospheric composition, radiative forcing, and climate change as a consequence of a
996 massive methane release from gas hydrates, Paleoceanography, 18(1), n/a-n/a, doi:10.1029/2002PA000757, 2003.
997 Schwietzke, S., Sherwood, O. A., Bruhwiler, L. M. P., Miller, J. B., Etiope, G., Dlugokencky, E. J., Michel, S. E., Arling, V.
998 A., Vaughn, B. H., White, J. W. C. and Tans, P. P.: Upward revision of global fossil fuel methane emissions based
999 on isotope database, Nature, 538(7623), 88–91, doi:10.1038/nature19797, 2016.
1000 Sherwood, O. A., Schwietzke, S., Arling, V. A. and Etiope, G.: Global Inventory of Gas Geochemistry Data from Fossil Fuel,
1001 Microbial and Burning Sources, version 2017, Earth Syst. Sci. Data, 9(2), 639–656, doi:10.5194/essd-9-639-2017,
1002 2017.
1003 Sperlich, P., Uitslag, N. A. M., Richter, J. M., Rothe, M., Geilmann, H., van der Veen, C., Röckmann, T., Blunier, T. and
1004 Brand, W. A.: Development and evaluation of a suite of isotope reference gases for methane in air, Atmos. Meas.
1005 Tech., 9(8), 3717–3737, doi:10.5194/amt-9-3717-2016, 2016.
1006 Stephenson, M. and Stickland, L. H.: Hydrogenase: The bacterial formation of methane by the reduction of one-carbon
1007 compounds by molecular hydrogen, Biochem. J., 27(5), 1517–1527, doi:10.1042/bj0271517, 1933.
1008 Thauer, R. K.: Biochemistry of methanogenesis: a tribute to Marjory Stephenson:1998 Marjory Stephenson Prize Lecture,
1009 Microbiology, 144(9), 2377–2406, doi:10.1099/00221287-144-9-2377, 1998.
1010 Tong, L. I., Chang, C. W., Jin, S. E. and Saminathan, R.: Quantifying uncertainty of emission estimates in National Greenhouse
1011 Gas Inventories using bootstrap confidence intervals, Atmos. Environ., 56, 80–87,
1012 doi:10.1016/j.atmosenv.2012.03.063, 2012.
1013 Townsend-Small, A., Disbennett, D., Fernandez, J. M., Ransohoff, R. W., Mackay, R. and Bourbonniere, R. A.: Quantifying
1014 emissions of methane derived from anaerobic organic matter respiration and natural gas extraction in Lake Erie,
1015 Limnol. Oceanogr., 61(S1), S356–S366, doi:10.1002/lno.10273, 2016.
1016 Turner, A. J., Frankenberg, C. and Kort, E. A.: Interpreting contemporary trends in atmospheric methane, Proc. Natl. Acad.
1017 Sci., 116(8), 2805–2813, doi:10.1073/PNAS.1814297116, 2019.
1018 Turner, D. B.: Workbook of Atmospheric Dispersion Estimates, U.S. Environmental Protection Agency. [online] Available
1019 from: https://nepis.epa.gov/Exe/ZyPDF.cgi/9101GKEZ.PDF?Dockey=9101GKEZ.PDF, 1969.
1020 U.S. EIA: Natural gas consumptions in the United States, [online] Available from:
1021 https://www.eia.gov/energyexplained/natural-gas/use-of-natural-gas.php (Accessed 16 June 2020), 2019.
1022 Van Ulden, A. P. and Wieringa, J.: Atmospheric boundary layer research at Cabauw, Boundary-Layer Meteorol., 78(1–2), 39–
1023 69, doi:10.1007/BF00122486, 1996.
1024 Umezawa, T., Brenninkmeijer, C. A. M., Röckmann, T., van der Veen, C., Tyler, S. C., Fujita, R., Morimoto, S., Aoki, S.,
1025 Sowers, T., Schmitt, J., Bock, M., Beck, J., Fischer, H., Michel, S. E., Vaughn, B. H., Miller, J. B., White, J. W. C.,
1026 Brailsford, G., Schaefer, H., Sperlich, P., Brand, W. A., Rothe, M., Blunier, T., Lowry, D., Fisher, R. E., Nisbet, E.
1027 G., Rice, A. L., Bergamaschi, P., Veidt, C. and Levin, I.: Interlaboratory comparison of δ13C and δD measurements
1028 of atmospheric CH4 for combined use of data sets from different laboratories, Atmos. Meas. Tech., 11(2), 1207–
1029 1231, doi:10.5194/amt-11-1207-2018, 2018.
1030 UNI MISKOLC and ETE: A register of all gas regulations and norms concerning the necessary gas quality for allowing the
1031 transport in the natural gas grid. [online] Available from: https://ec.europa.eu/energy/intelligent/projects/sites/iee-
1032 projects/files/projects/documents/redubar_a_register_of_all_gas_regulations.pdf, 2008.

US Census Bureau: U.S. and World Population Clock, [online] Available from: https://www.census.gov/popclock/ (Accessed 20 June 2020), 2020.
Weller, Z., Hamburg, S. P. and von Fischer, J. C.: A national estimate of methane leakage from pipeline mains in natural gas local distribution systems, Environ. Sci. Technol., doi:10.1021/acs.est.0c00437, 2020.
Weller, Z. D., Roscioli, J. R., Daube, W. C., Lamb, B. K., Ferrara, T. W., Brewer, P. E. and von Fischer, J. C.: Vehicle-Based Methane Surveys for Finding Natural Gas Leaks and Estimating Their Size: Validation and Uncertainty, Environ. Sci. Technol., acs.est.8b03135, doi:10.1021/acs.est.8b03135, 2018.
Weller, Z. D., Yang, D. K. and von Fischer, J. C.: An open source algorithm to detect natural gas leaks from mobile methane survey data, edited by M. Mauder, PLoS One, 14(2), e0212287, doi:10.1371/journal.pone.0212287, 2019.
West, J. J., Fiore, A. M., Horowitz, L. W. and Mauzerall, D. L.: Global health benefits of mitigating ozone pollution with methane emission controls., Proc. Natl. Acad. Sci. U. S. A., 103(11), 3988–93, doi:10.1073/pnas.0600201103, 2006.
Xu, L. and Jiang, C.: Initial desorption characterization of methane and carbon dioxide in coal and its influence on coal and gas outburst risk, Fuel, 203, 700–706, doi:10.1016/J.FUEL.2017.05.001, 2017.
Yacovitch, T. I., Herndon, S. C., Roscioli, J. R., Floerchinger, C., McGovern, R. M., Agnese, M., Pétron, G., Kofler, J., Sweeney, C., Karion, A., Conley, S. A., Kort, E. A., Nähle, L., Fischer, M., Hildebrandt, L., Koeth, J., McManus, J. B., Nelson, D. D., Zahniser, M. S. and Kolb, C. E.: Demonstration of an Ethane Spectrometer for Methane Source Identification, Environ. Sci. Technol., 48(14), 8028–8034, doi:10.1021/es501475q, 2014.
Yacovitch, T. I., Herndon, S. C., Pétron, G. P., Kofler, J., Lyon, D., Zahniser, M. S. and Kolb, C. E.: Mobile Laboratory Observations of Methane Emissions in the Barnett Shale Region, , doi:10.1021/es506352j, 2015.
Yacovitch, T. I., Neininger, B., Herndon, S. C., Van der Gon, H. D., Jonkers, S., Hulskotte, J., Roscioli, J. R. and Zavala-Araiza, D.: Methane emissions in the Netherlands: The Groningen field, Elem Sci Anth, 6(1), 57, doi:10.1525/elementa.308, 2018.
Zavala-Araiza, D., Lyon, D. R., Alvarez, R. A., Davis, K. J., Harriss, R., Herndon, S. C., Karion, A., Kort, E. A., Lamb, B. K., Lan, X., Marchese, A. J., Pacala, S. W., Robinson, A. L., Shepson, P. B., Sweeney, C., Talbot, R., Townsend-Small, A., Yacovitch, T. I., Zimmerle, D. J. and Hamburg, S. P.: Reconciling divergent estimates of oil and gas methane emissions., Proc. Natl. Acad. Sci. U. S. A., 112(51), 15597–602, doi:10.1073/pnas.1522126112, 2015.
Zazzeri, G., Lowry, D., Fisher, R. E., France, J. L., Lanoisellé, M. and Nisbet, E. G.: Plume mapping and isotopic characterisation of anthropogenic methane sources, Atmos. Environ., 110, 151–162, doi:10.1016/j.atmosenv.2015.03.029, 2015.
Zhao, W., Zhang, T., Wang, Y., Qiao, J. and Wang, Z.: Corrosion Failure Mechanism of Associated Gas Transmission Pipeline., Mater. (Basel, Switzerland), 11(10), doi:10.3390/ma11101935, 2018.
Zimmerle, D. J., Williams, L. L., Vaughn, T. L., Quinn, C., Subramanian, R., Duggan, G. P., Willson, B., Opsomer, J. D., Marchese, A. J., Martinez, D. M. and Robinson, A. L.: Methane Emissions from the Natural Gas Transmission and Storage System in the United States, Environ. Sci. Technol., 49(15), 9374–9383, doi:10.1021/acs.est.5b01669, 2015.
Zimnoch, M., Necki, J., Chmura, L., Jasek, A., Jelen, D., Galkowski, M., Kuc, T., Gorczyca, Z., Bartyzel, J. and Rozanski, K.: Quantification of carbon dioxide and methane emissions in urban areas: source apportionment based on atmospheric observations, Mitig. Adapt. Strateg. Glob. Chang., 24(6), 1051–1071, doi:10.1007/s11027-018-9821-0, 2019.

Table 1: Natural gas distribution network CH_4 emission categories

Class	CH_4 Enhancement (ppm)	Equivalent Emission Rate (L min^{-1})	Equivalent Emission Rate (≈ kg hr^{-1})	LI Location Colour (Figure 1, Figure 2, and Figure S14)
High	>7.6	>40	>1.7	Red
Medium	1.6-7.59	6 - 40	0.3 – 1.7	Orange
Low	0.2-1.59	0.5 - 6	0.0 – 0.3	Yellow

1144 **Table 2- Measurements and results summaries across the study area, inside the ring in Utrecht and north Elbe in Hamburg**

Study Area				Utrecht (inside the Ring)	Hamburg (North Elbe)
≈ km street driven		Total km driven		1,000 km	1,800 km
		Driven once		220 km	900 km
		Driven more than once		780 km	900 km
≈ km street covered		Total km covered		450 km	1,200 km
		covered once		230 km	900 km
		covered more than once		220 km	300 km
LIs and emissions		Total number		81 LIs	145 LIs
		LI density		5.6 km covered LI^{-1}	8.4 km covered LI^{-1}
		Total emission rate		290 L min^{-1}	490 L min^{-1}
		Average emission rate per LI		3.6 L min^{-1} LI^{-1}	3.4 L min^{-1} LI^{-1}
		Total emission rate per year		107 t yr^{-1}	180 t yr^{-1}
LIs visited	Once	Number		16 LIs	45 LIs
		Emissions		26 L min^{-1}	68 L min^{-1}
		Average emission rate per LI		1.6 L min^{-1} LI^{-1}	1.5 L min^{-1} LI^{-1}
	More than once	Number		65 LIs	100 LIs
		Emissions		264 L min^{-1}	423 L min^{-1}
		Average emission rate per LI		4.1 L min^{-1} LI^{-1}	4.2 L min^{-1} LI^{-1}
Total LIs categorized based on von Fischer et al. (2017) categories	High (>40 L min^{-1})	Number		1 LI	2 LIs
		Emissions		102 L min^{-1}	145 L min^{-1}
		Average emission rate per LI		101.5 (L min^{-1} LI^{-1})	72.4 L min^{-1} LI^{-1}
		% of emissions		35 % of total emissions	30 % of total emissions
	Medium (6-40 L min^{-1})	Number		6 LIs	16 LIs
		Emissions		84 L min^{-1}	176 L min^{-1}
		Average emission rate per LI		14.0 L min^{-1} LI^{-1}	11 L min^{-1} LI^{-1}
		% of emissions		30 % of total emissions	36 % of total emissions
	Low (0.5-6 L min^{-1})	Number		74 LIs	127 LIs
		Emissions		105 L min^{-1}	169 L min^{-1}
		Average emission rate per LI		1.4 L min^{-1} LI^{-1}	1.3 L min^{-1} LI^{-1}
		% of emissions		36 % of total emissions	35 % of total emissions
Total LIs categorized based on OSM road classes	Level 1	Number		6 LIs	29 LIs
		Emissions		5 L min^{-1}	68 L min^{-1}
		Average emission rate per LI		0.76 L min^{-1} LI^{-1}	2.3 L min^{-1} LI^{-1}
	Level 2	Number		16 LIs	34 LIs
		Emissions		145 L min^{-1}	99 L min^{-1}
		Average emission rate per LI		9.0 L min^{-1} LI^{-1}	2.9 L min^{-1} LI^{-1}
	Level 3	Number		3 LIs	23 LIs
		Emissions		10 L min^{-1}	43 L min^{-1}
		Average emission rate per LI		3.4 L min^{-1} LI^{-1}	1.9 L min^{-1} LI^{-1}
	Residential	Number		45 LIs	52 LIs
		Emissions		93 L min^{-1}	274 L min^{-1}
		Average emission rate per LI		2.1 L min^{-1} LI^{-1}	5.3 L min^{-1} LI^{-1}
	Unclassified	Number		11 LIs	7 LIs
		Emissions		38 L min^{-1}	6 L min^{-1}
		Average emission rate per LI		3.4 L min^{-1} LI^{-1}	0.8 L min^{-1} LI^{-1}
Attribution	C_2:C_1 ratio analysis	Fossil (Inc. combustion)	% of emissions	93 % of total emissions	64 % of total emissions
			% of LIs	69 % of LIs	33 % of LIs
		Microbial	% of emissions	6 % of total emissions	25 % of total emissions
			% of LIs	10 % of LIs	20 % of LIs
		Unclassified	% of emissions	1 % of total emissions	11 % of total emissions
			% of LIs	21 % of LIs	47 % of LIs
	$\delta^{13}C$ and δD analysis	Fossil	% of emissions	----------	79 % of total emissions
			% of LIs	----------	38 % of LIs
		Microbial	% of emissions	----------	20 % of total emissions
			% of LIs	----------	54 % of LIs
		Other	% of emissions	----------	1 % of total emissions
			% of LIs	----------	8 % of LIs (Pyrogenic)

	CH_4:CO_2 ratio analysis	Combustion	% of emissions	2 %	10 %
			% of LIs	7 %	17 %
		Other	% of emissions	98 %	90 %
			% of LIs	93 %	83 %
	C_2:C_1 ratio, CH_4:CO_2 ratio, and $\delta^{13}C$ - δD analyses	Fossil	% of emissions	73 %	48 %
			% of LIs	43 %	31 %
		Combustion	% of emissions	2 %	10 %
			% of LIs	7 %	17 %
		Microbial	% of emissions	8 %	35 %
			% of LIs	4 %	33 %
		Unclassified	% of emissions	16 %	7 %
			% of LIs	46 %	19%
Average emission rate per km driven				0.29 L min^{-1} km^{-1}	0.27 L min^{-1} km^{-1}
km driven / total LIs				12.5 km LI^{-1}	12.36 km LI^{-1}
Emission factors to scale-up emissions per km covered				0.64 L min^{-1} km^{-1}	0.40 L min^{-1} km^{-1}
km covered per LIs		km covered / total LIs		5.6 km LI^{-1}	8.4 km LI^{-1}
		km covered / red LIs		454.8 km LI^{-1}	611.4 km LI^{-1}
		km covered / orange LIs		75.8 km LI^{-1}	76.4 km LI^{-1}
		km covered / yellow LIs		6.1 km LI^{-1}	9.6 km LI^{-1}
km road from OSM (≈ km pipeline)				≈ 650 km	≈ 3000 km
Up-scaled methane emissions to total roads				420 L min^{-1} (≈150 t yr^{-1})	1,200 L min^{-1} (≈440 t yr^{-1})
Bootstrap emission rate estimate and error				420 ± 120 L min^{-1}	1,200 ± 170 L min^{-1}
Population in study area				≈ 0.28 million	≈ 1.45 million
Average LIs emissions per capita (kg yr^{-1} $capita^{-1}$)				0.54 ± 0.15	0.31 ± 0.04
Yearly natural gas consumption				≈ 0.16 bcm yr^{-1}	≈ 0.75 bcm yr^{-1}
Fossil emission factors	C_2:C_1 ratio attribution analysis		Average emission rate per km gas pipeline	0.60 ± 0.2 L min^{-1} km^{-1}	0.26 ± 0.04 L min^{-1} km^{-1}
			Average emission rates per capita	0.50 ± 0.14 kg yr^{-1} $capita^{-1}$	0.20 ± 0.03 kg yr^{-1} $capita^{-1}$
	$\delta^{13}C$ and δD attribution analysis		Average emission rates per km gas pipeline	----------	0.32 ± 0.05 L min^{-1} km^{-1}
			Average emission rates per capita	----------	0.25 ± 0.04 kg yr^{-1} $capita^{-1}$
	C_2:C_1 ratio, CH_4:CO_2 ratio, and $\delta^{13}C$ - δD analyses		Average emission rates per km gas pipeline	0.47 ± 0.14 L min^{-1} km^{-1}	0.19 ± 0.03 L min^{-1} km^{-1}
			Average emission rates per capita	0.39 ± 0.11 kg yr^{-1} $capita^{-1}$	0.15 ± 0.02 kg yr^{-1} $capita^{-1}$
			Average emission rates / yearly consumption	0.10 – 0.12 %	0.04 – 0.07 %

Table 3- CH_4 Emissions from larger facilities in Utrecht and Hamburg estimated with the Gaussian Plume model

Facility	Emission rate (t yr^{-1})
Utrecht	
Waste Water Treatment Plant (52.109791° N, 5.107605° E)	160 ± 90
Hamburg	
F: Compost and Soil Company (53.680233° N, 10.053751° E)	70 ± 50
Upstream D1: 53.468774° N,10.184481° E (separator) D2: 53.468443° N,10.187408° E (storage tanks) D3: 53.466694° N,10.180647° E (oil well)	 D1: 4.5 ± 3.7 D2: 5.2 ± 3.0 D3: 4.8 ± 4.0

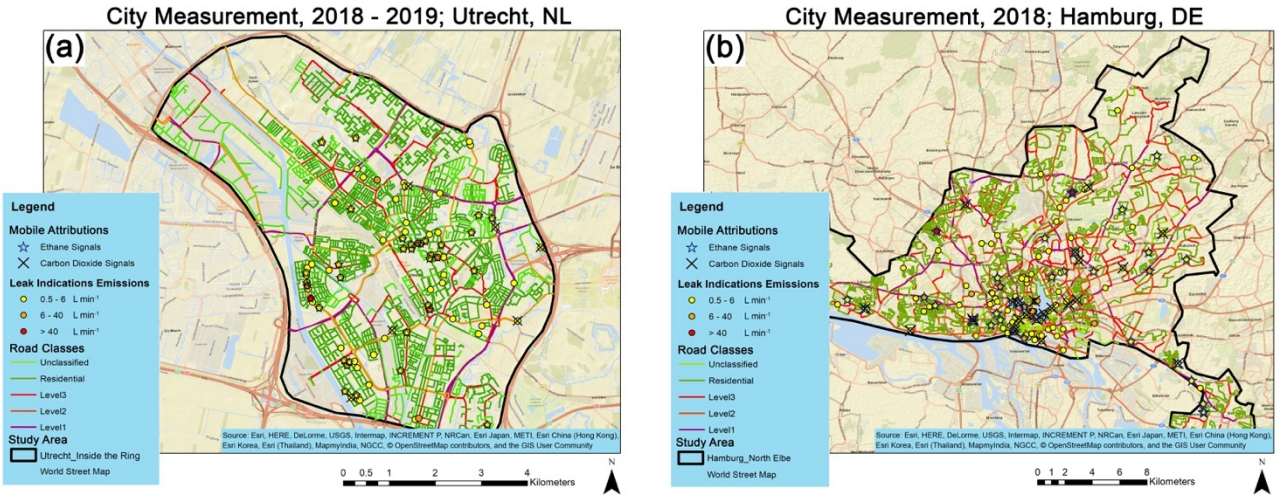

Figure 1: Locations of significant LIs for the categories on different street classes in (a) Utrecht and (b) Hamburg. Road colors indicate the street classes according to the OSM. Black polygons show urban study areas.

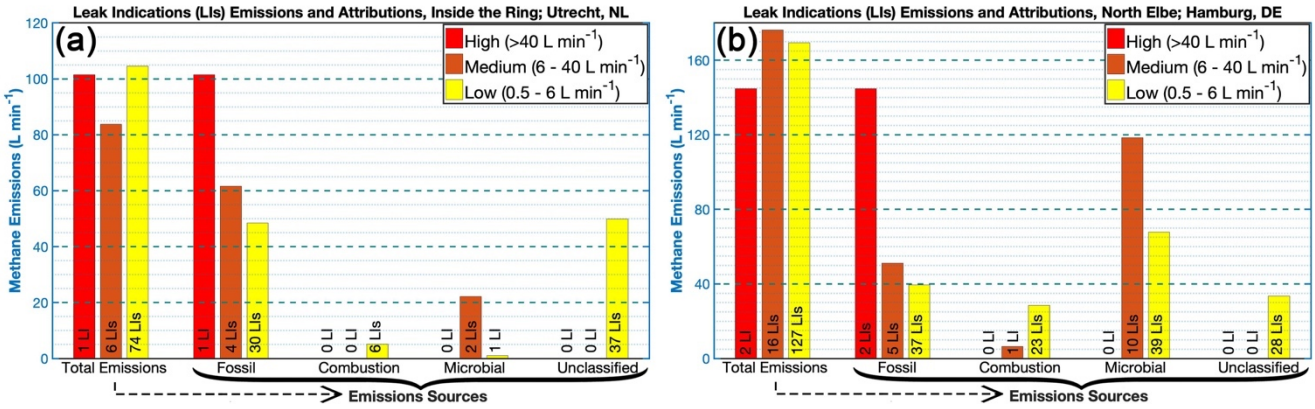

Figure 2: Total CH_4 emission rates from different sources in (a) Utrecht and (b) Hamburg; the arrow shows how the emissions are attributed to different sources

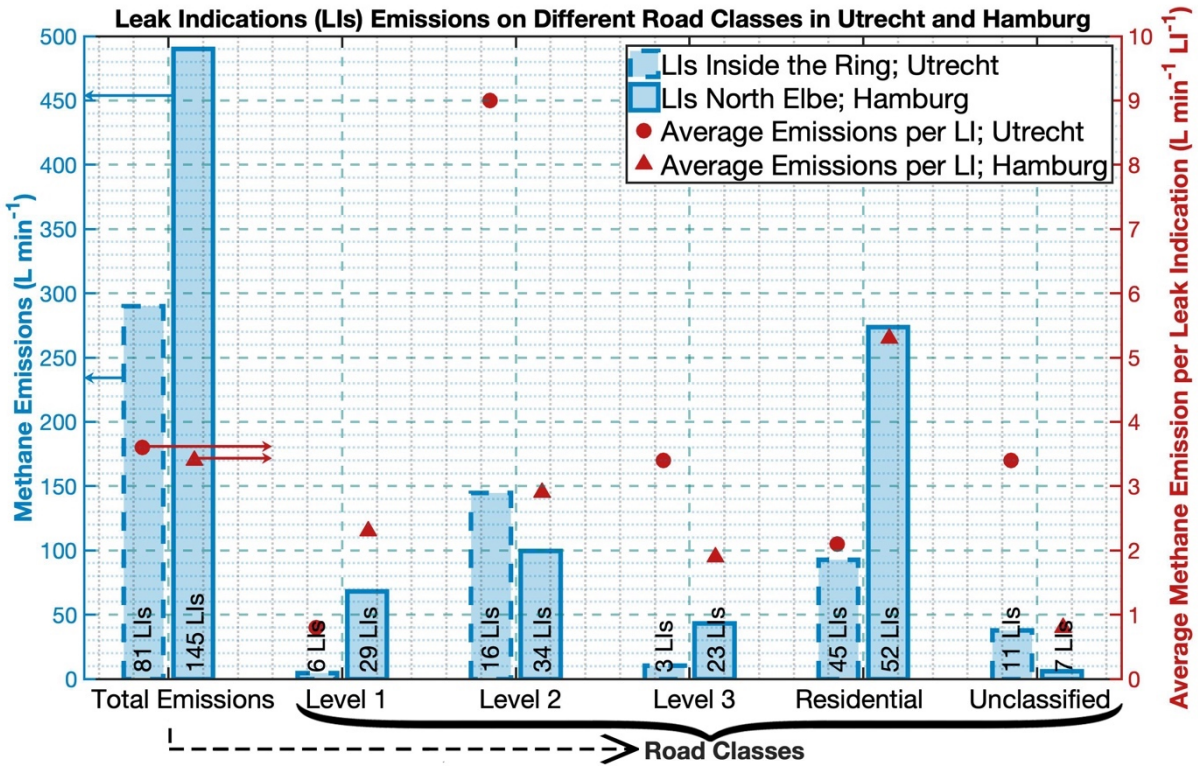

Figure 3: Total CH_4 emissions in Utrecht and Hamburg; the arrow shows how the total emissions are distributed on different road classes

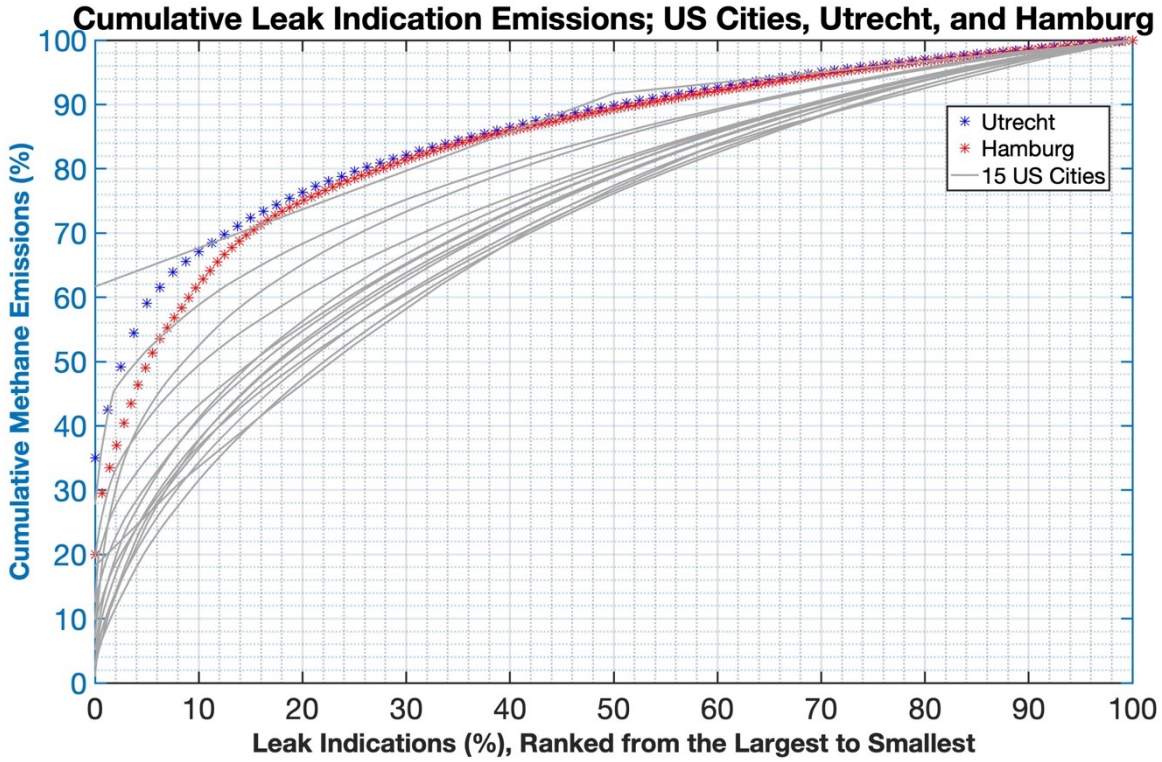

Figure 4: Cumulative plot of CH_4 emissions across US cities, Utrecht, and Hamburg; datasets for the US cities are from Weller et al. (2019)

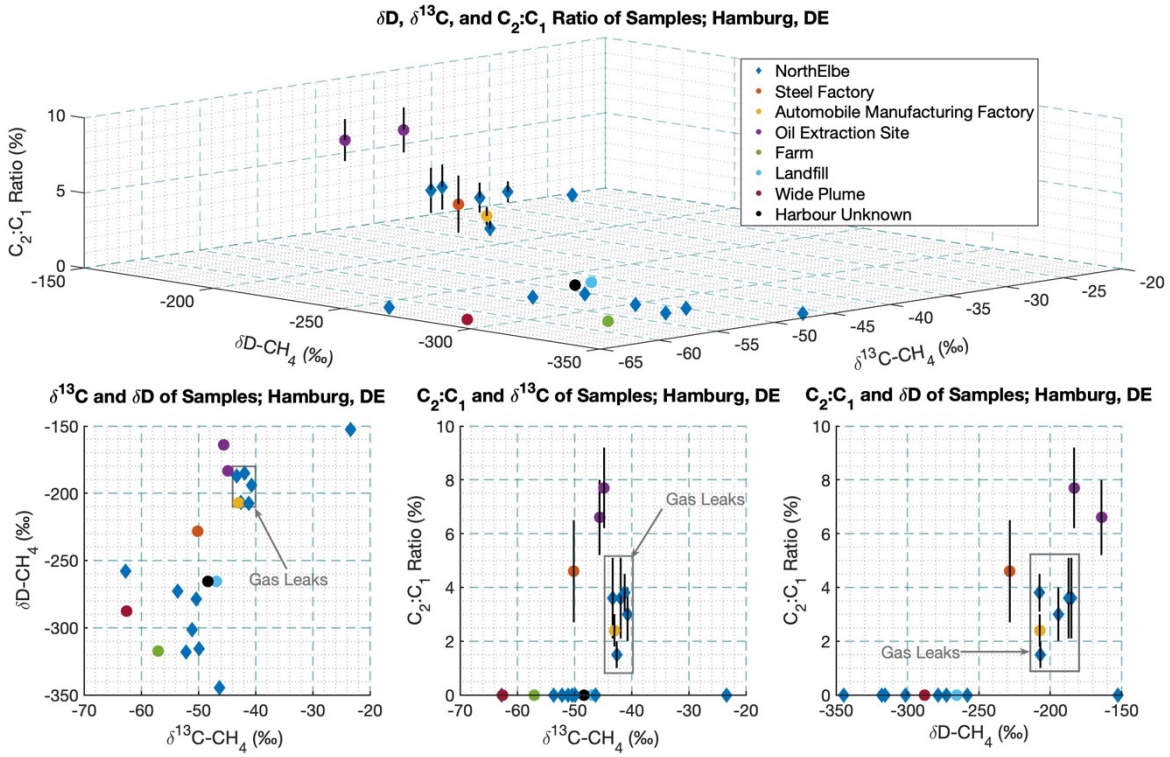

Figure 5: Results from the attribution measurements in Hamburg: C_2:C_1 ratios, and isotopic signatures ($\delta^{13}C$ and δD) of collected air samples; measurement uncertainties in $\delta^{13}C$ is 0.05 - 0.1 ‰ and in δD is 2 - 5 ‰

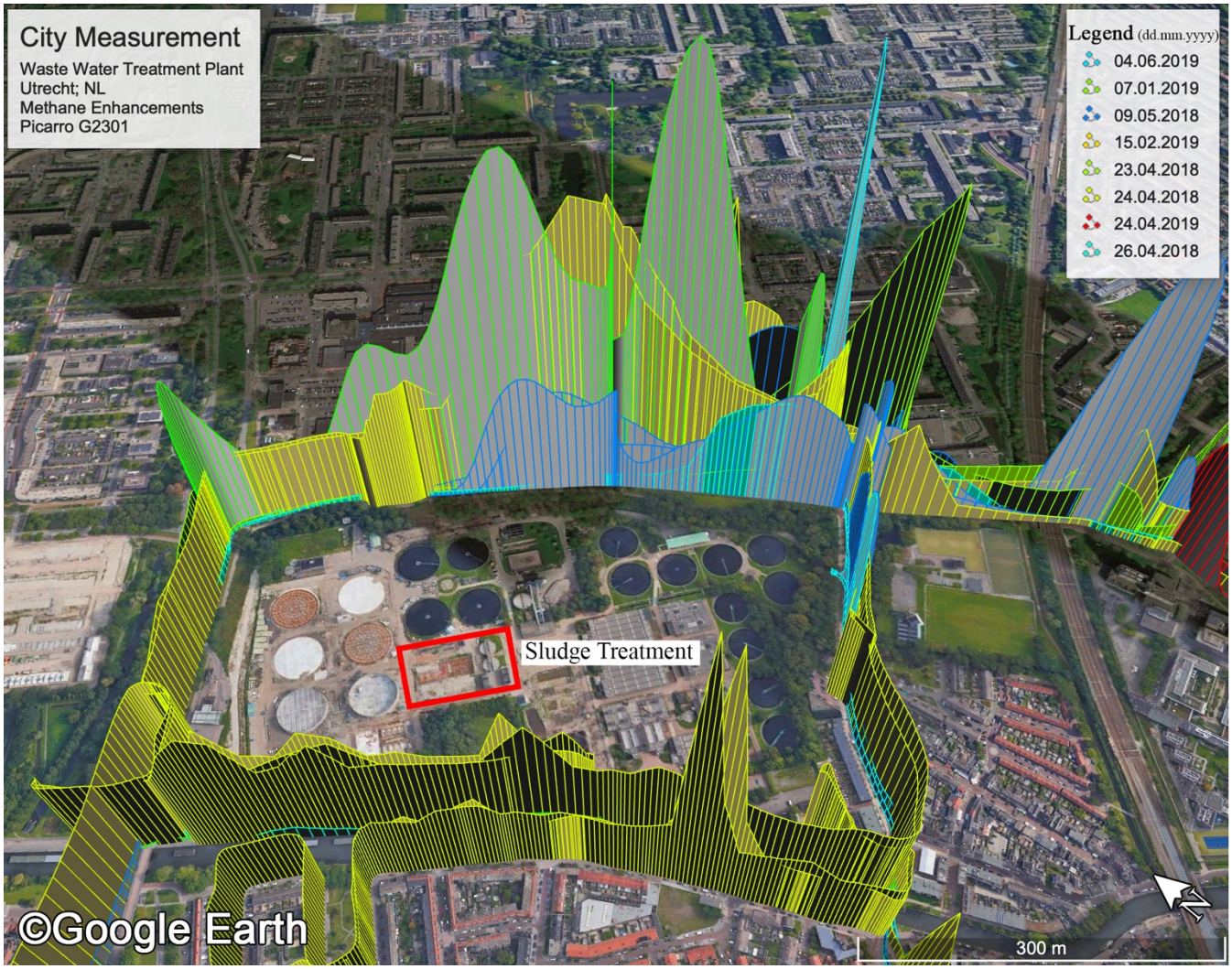

Figure 6: CH_4 enhancements measured downwind waste water treatment plant on Brailledreef street and later used for quantifications from this facility in Utrecht; the centre of the area where the sludge treatment is located was considered as the effective CH_4 emission source, the plumes are plotted on the same scale and max CH_4 enhancement is ≈ 0.3 ppm

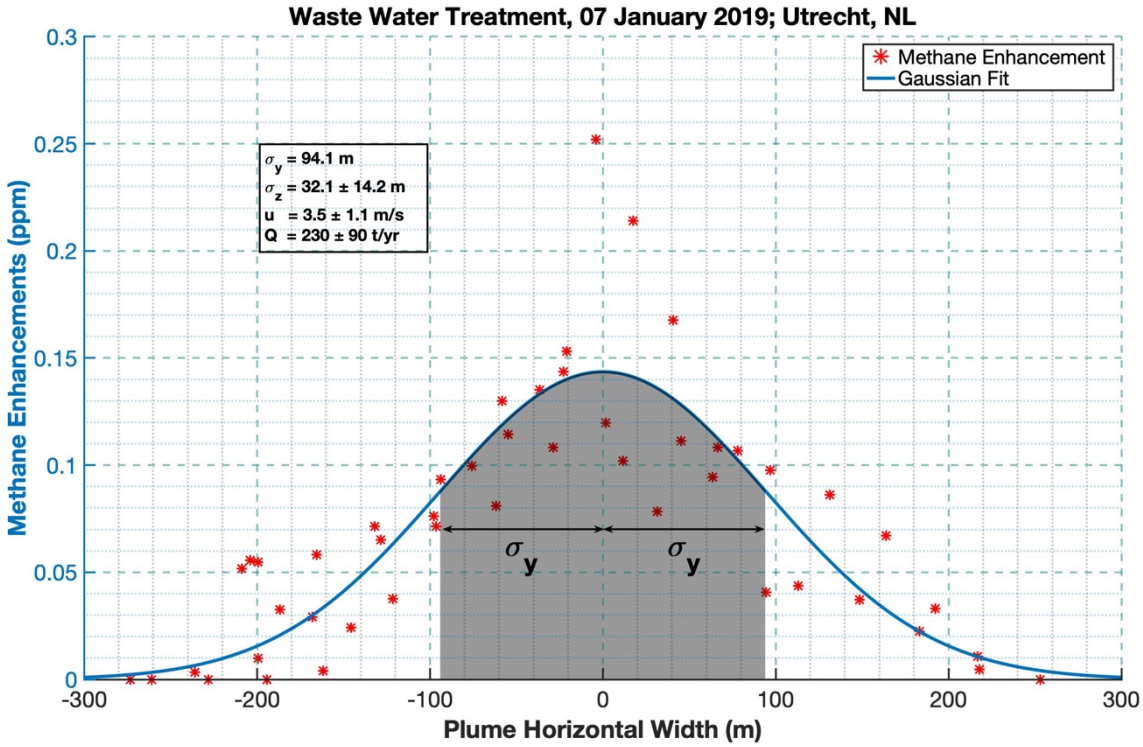

Figure 7: Gaussian curve fitted to some transects downwind the waste water treatment plant in Utrecht